Design Study for the JET Diagnostic System: "Quasi-Continuous Laser Scattering[++)]"

H.Röhr, K.-H.Steuer
K.Hirsch[+)], H.Salzmann[+)]

IPP III/55
IPF 8o-2

January 198o

MAX-PLANCK-INSTITUT FÜR PLASMAPHYSIK

8046 GARCHING BEI MÜNCHEN

MAX-PLANCK-INSTITUT FÜR PLASMAPHYSIK

GARCHING BEI MÜNCHEN

Design Study for the JET Diagnostic System: "Quasi-Continuous Laser Scattering[++)]"

H.Röhr, K.-H.Steuer
K.Hirsch[+)], H.Salzmann[+)]

IPP III/55
IPF 8o-2

January 198o

[+)] Institut für Plasmaforschung
der Universität Stuttgart

[++)] This work was done under article 14
of JET Statutes (contract Number B-GI-4o2)

Die nachstehende Arbeit wurde im Rahmen des Vertrages zwischen dem Max-Planck-Institut für Plasmaphysik und der Europäischen Atomgemeinschaft über die Zusammenarbeit auf dem Gebiete der Plasmaphysik durchgeführt.

Abstract

The design study for a quasi-continuous Thomson scattering system for JET capable of measuring the electron temperature throughout the discharge time is reported. The arrangement is based on a 8° forward scattering geometry. Different possible laser systems are compared. The chosen laser is a 100 Hz repetition rate Q-switched neodymium laser emitting at least 1 J unpolarized per pulse. Silicon avalanche photodiodes are used as detectors. The merits of these detectors for scattering experiments are discussed and signal-to-noise considerations are given.

Contents

A) Scope of the proposed experiment

The objective of the design study is to assess the requirements of a quasi-continuous Thomson scattering system for JET which could be used to measure the electron temperature throughout the discharge period. The improvement on standard Thomson scattering is primarily afforded by the development of reliable multipulse laser systems which emit up to 100 pulses/s at sufficiently high energies and sufficiently low beam divergence. The goal is to measure the scattered spectrum from each individual laser pulse and to derive the electron temperature within an accuracy of 10 %. The time development of the density can be measured as well. Radial temperature and density profiles in the equatorial plane can be scanned.

B) Scientific principles

I. Possible scattering arrangements

There are two scattering arrangements possible for JET, large angle scattering ($\sim 90^{\circ}$) and small angle scattering ($\sim 10^{\circ}$). In the case of 90° scattering the laser beam would be passed vertically through the torus. In order to collect as much scattered light as possible, one would use large-aperture collection optics. Apertures of up to 1 : 6 can be obtained by using the large middle port of the rigid torus section. Figure 1 shows schematically the scattering arrangement and indicates the accessible plasma region.

In the case of small angle scattering the laser beam is passed tangentially through the torus in the equatorial plane. Figure 2 shows a top and a side view of the beam paths inside the torus. A scattering volume at the centre of the plasma can be observed at a maximum angle of 9°. A radial scan is possible by shifting the focusing

and observation optics.

The scattered spectrum is Doppler-broadened by the thermal velocities of the electrons. The half-width, which in the non-relativistic case is proportional to

$$\text{FWHM} \propto \sin \Theta/2 \sqrt{T_e} \qquad (1)$$

(Θ = scattering angle), yields the electron temperature T_e.

Because of this relation the scattered spectrum becomes fairly broad for high temperature at 90°, e.g. FWHM = 4400 Å for 10 keV (λ_o = 1.06 μm). This fact requires achromatic collection and transmission optics, a spectrometer of high transmission over a broad spectral region and a detector sensitive over the whole spectrum or different matched detectors. Furthermore, the plasma background radiation impinging on the detector is intense owing to the large bandwidth of the spectral channels. Compared with 90° scattering, the forward scattering arrangement, to be discussed in detail in the following, offers several advantages:

1. The spectral width of the scattered light is much smaller than in the case of 90° scattering:

   FWHM = 490 Å for 10 keV (λ_o = 1.06 μm, Θ = 8°).

   The requirements imposed on the degree of achromatic correction of the collection and transmission optics are thus much less stringent.
   Furthermore, there is less background radiation than in the 90° case (even taking into account the larger depth of plasma which is observed in forward scattering).

2. In forward scattering only low f-number-optics are allowed (the spectral shape varies strongly with scattering angle). The collection optics therefore become much simpler.

3. Though the f-numbers are smaller than for 90° scattering, more scattered photons are collected since the observed scattering volume becomes longer.

4. As will be shown later in detail (Appendix 2), the relativistic effects are small and may even be neglected in the evaluation of the scattered light spectra for temperatures $T_e < 10$ keV. This is not the case for 90° scattering.

5. It is possible to measure radial profiles of T_e and n_e in the equatorial plane by shifting the scattering volume between the discharges .

In view of the foregoing we shall treat in detail a forward scattering scheme. We shall then compare the results for this arrangement with those for the 90° setup. It is found that the signal - to - noise ratios for the case of forward scattering are better than those for a 90° arrangement.

II. Choice of laser

We estimate the necessary laser power for two scattering angles $\theta = 15^{\circ}$ and $\theta = 8^{\circ}$ and compare the results with those of a 90° scattering experiment. For the calculation of the laser energy necessary for a given signal-to-noise ratio the scattering geometry, the plasma background radiation and the noise figure of detectors must be known.

a) Forward scattering geometry

The laser beam is focused to a diameter of $\Delta x \leq 10$ mm and the length of the observed plasma is 800 cm. A reasonable cross-section of the observation beam is 1×2 cm^2 at the intersection with the laser beam. At 15° we can use a solid angle of 10^{-2} sterad for detection. At 8° two observation beams with 0.8×10^{-2} sterad each which are symmetric to the horizontal plane are possible in principle. In the following calculations it is

assumed that only one observation beam is used. The lengths l of the scattering volumes are 2.0cm/sin θ = 7.7 cm (15°) and 14.4 cm (8°) (see fig. 3).

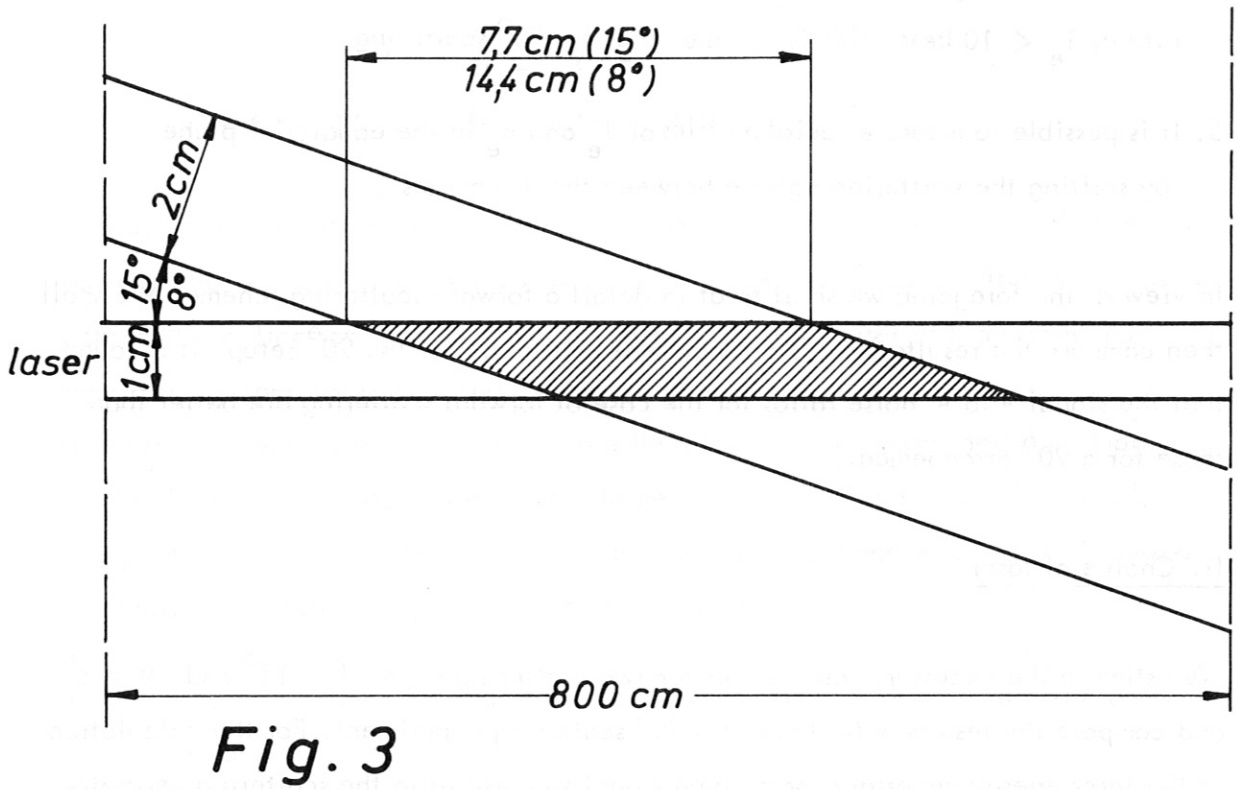

Fig. 3

Fig. 3: Definition of scattering volume by intersection of laser and observation beams.

b) Scattered power

For signal - to - noise estimates one has to know the powers incident on the detector. We assume an overall transmission factor T = 0.1 for the observation system. The spectral width of one channel may be 1/6 the half-width of the scattered spectrum. An average channel then receives 1/12 of the scattered light impinging on the observation optics. This corresponds to a channel at the half-width of the spectrum.

This representative channel receives the fraction Σ of the laser power at the focus

$$\Sigma = \frac{\sigma_{Th}}{12} \cdot n_e \cdot T \cdot l \cdot \Delta\Omega \qquad (2)$$

which is

$$\Sigma\ (15^\circ) = n_e \cdot 5.1 \times 10^{-29}\ cm^3$$

$$\Sigma\ (8^\circ) = n_e \cdot 7.6 \times 10^{-29}\ cm^3$$

The scattered power on the detector is Σ x laser power.

The signal - to - noise ratio will be determined by the noise of the detector (dark current), by the shot noise of electrons produced within the detector by plasma background and scattered radiation, and by noise due to the internal amplification mechanism. Dark currents are negligible when multipliers are used but must be taken into account when avalanche diodes are used.

c) Plasma background radiation

An estimate of the background radiation is given by the bremscontinuum of a hydrogen plasma.

Emission coefficients are taken from Glasstone-Loveberg/1/ and Eberhagen-Lünow/2/. The emission of the plasma (bremscontinuum) at 4 keV and $1 \times 10^{13} cm^{-3}$ is listed in Table I for different wavelengths which are emitted by powerful lasers. The half-widths of the scattered spectra at 4 keV for $\Theta = 15^\circ$ and 8° as well as the representative channel widths $\Delta\lambda$ are presented in Table I.

Laser		Nd	Ruby	Dye	Cu	XeF	KrF
λ [Å]		10600	6943	6000	5100	3500	2500
ε [W/Å cm^3 sr]		1.1×10^{-12}	2.3×10^{-12}	3.1×10^{-12}	4.0×10^{-12}	8.3×10^{-12}	16.1×10^{-12}
FWHM [Å]	15°	576	377	326	277	190	136
	8°	308	202	174	148	102	73
$\Delta\lambda$ [Å]	15°	96	63	54.3	46.2	31.7	22.6
	8°	51.3	33.5	29	24.7	16.9	12.1

Table I

To estimate the plasma radiation the observed volume has to be calculated. This volume is taken as the cross-section of the waist of the observation beam times the thickness of the plasma along the line of sight of the collection optics (approx. 8 m in the case of forward scattering). This estimate gives, of course, for both forward scattering angles the same effective plasma volume of 1600 cm^3. The solid angle dΩ is taken as that of the collection optics.

The bremscontinuum yields only a lower bound for the emissionactually observed . The enhancement factor K is strongly dependent on the individual plasma machine which is considered and no exact predictions can be made. Present-day tokamaks generally report enhancement factors of between 10 and 100 in the visible part of the spectrum. There is a tendency for K to decrease at longer wavelengths (measurement in Pulsator). This is not very surprising since the resonance lines of impurities are mainly located in the ultraviolet (one of the arguments for scattering experiments at 1 μm).

In our estimate we assume a wavelength - independent enhancement factor of K = 100.

Table II shows values of the plasma radiation power P per scattering channel with K = 100 for (T_e = 4 keV; $n_e = 1 \times 10^{13}$ cm^{-3}); the transmission factor is T = 0.1.

λ [Å]		10600	6943	6000	5100	3500	2500
P [W]	15°	1.7×10^{-8}	2.3×10^{-8}	2.7×10^{-8}	3×10^{-8}	4.2×10^{-8}	5.8×10^{-8}
	8°	7.2×10^{-9}	9.9×10^{-9}	1.2×10^{-8}	1.3×10^{-8}	1.8×10^{-8}	2.5×10^{-8}

Table II

d) Laser energies required

Using the formula (3), obtained from equation 22 (Sec. C VI)

$$Lt = \frac{(S/N)^2 \cdot h\nu}{2\eta\Sigma}\left[1+\sqrt{1+\frac{8\eta t}{(S/N)^2\, h\nu}\left(P+\frac{NEP^2\eta}{2h\nu}\right)}\right] \qquad (3)$$

which combines laser power L, the noise - equivalent - power (NEP), plasma radiation power P, quantum efficiency, gating time t, and the quantitiy Σ as defined in B IIb and finally the required signal - to - noise ratio S/N one gets the necessary laser energies for S/N = 10 listed in Table 3. Numbers of scattered (n_s) as well as plasma light quanta (n_{pl}) arealso listed in Table 3.

λ [Å]		10600	6943	6000	5100	3500	2500
t [ns]		50	20	1000	25	20	20
η		0.3 *	0.05	0.1	0.2	0.25	0.25
NEP $\left[\frac{W}{\sqrt{Hz}}\right]$		10^{-13}	10^{-15}	10^{-15}	10^{-15}	10^{-15}	10^{-15}
Lt [Ws]	15°	2.8	2.1	8.6	1.3	1.4	2.0
	8°	1.4	1.1	3.9	0.6	0.7	1.0
n_s	15°	7556	3735	13329	1665	1310	1303
	8°	5800	2946	9061	1166	942	940
n_{pl}	15°	4570	1620	82167	1940	1491	1471
	8°	1935	697	36519	776	639	634

Table III

* See page 9.

* Using avalanche diodes at 10600 Å one has to consider an excess noise factor $F \approx 10$ which is caused by the avalanche effect (see Sec.C VI). This additional noise has been taken into account by changing η to η/F in formula (3).

We compare these values with those of a 90° scattering experiment ($\Delta\Omega = 2 \times 10^{-2}$ sterad, scattering volume 1 x 1 x 2.5 cm^3, plasma depth 250 cm) and find that the required laser energy is about 4 times as high as it is in a 8° scattering experiment (Table 4). In addition, the energy in a 90° scattering experiment has to be in one polarization, whereas a laser for small angle scattering is allowed to be unpolarized.

λ [Å]	Δt [ns]	15° $\Delta\Omega = 10^{-2}$ sr $l = 7.7$ cm	8° $\Delta\Omega = 0.8 \times 10^{-2}$ sr $l = 14.4$ cm	90° $\Delta\Omega = 2 \times 10^{-2}$ sr $l = 2.5$ cm
		can be unpolarized	*can be unpolarized*	*must be polarized*
10 600	50	2.8 J	1.4 J	5.6 J
6943	20	2.1 J	1.1 J	4.1 J
6000	1000	8.6 J	3.9 J	18 J
5100	25	1.3 J	0.6 J	2.6 J
3500	20	1.4 J	0.7 J	3 J
2500	20	2 J	1 J	4.2 J

Table IV

The dependence of necessary laser energies on density is shown in Fig. 4.

e) Discussion of different lasers

The required laser energy for scattering measurements in JET is appr. 2 J at 15° and appr.1 J at 8°.This yields at 100 Hz average laser powers of 100 to 200 W, and requires input powers of a few tens of kW. Lasers which may fulfill these requirements are Nd-YAG, Nd-glass and exciplex lasers such as XeF or KrF.

1. YAG laser

The laser material most commonly used to produce high average output powers is Nd-YAG. This is because the material has good thermal and mechanical properties with a very high gain coefficient which yields low laser thresholds (4 level system). This makes YAG-lasers ideal for operating at a high repetition rate. Average powers of several hundred watts cw are already available from such commercial systems. However,when it comes to operating Nd-YAG lasers in the Q-switched mode, the maximum output pulse which can be obtained from one oscillator is severely limited by superradiance in the laser material. This is a direct consequence of the high gain coefficient of the material and it effectively means that not more than 400 millijoules can be stored in a 3" x 1/4" YAG rod. Unfortunately, it is just not possible to extract all of this energy from an oscillator in a single Q-switched pulse and in general the optimal coupling for maximum overall efficiency restricts the Q-switched output pulse energy to approximately one-third of the stored energy. This can in fact be increased to approximately half of the stored energy by increasing the coupling coefficient of the laser resonator, but this reduces the overall efficiency, thus leading to higher power supply drive requirements and consequently lower flashtube life.

The normal way to increase the individual pulse energy available from a Q-switched

YAG system is therefore to use amplifiers after the oscillator. For input energies of above 400 mJ per square centimetre into a YAG rod used as an amplifier, the amplifier operates in the saturated region and consequently more than 80 % of the stored energy is extracted and added to the input energy from the oscillator. One might thus expect a 3" x 1/4" YAG oscillator followed by a 4" x 1/4" and a 4" x 3/8" amplifier to produce a pulse output energy in excess of 1 J.

Further complications arise with such systems when operated at high repetition rates. In particular, the high average input power from the exciting lamps causes strain birefringence in the laser rod. This means that there is some polarization rotation as the laser beam passes through the rods. Firstly this reduces the output available from the laser oscillator since a certain amount of the energy is coupled out by the polarizer rather than by the output mirror of the laser. Typically for a 3" x 1/4" YAG laser oscillator, the output energy in a single polarization begins to decrease for pulse repetition rates above 20 Hz. J K Lasers (Rugby UK) have carried out measurements at repetition rates up to 50 Hz, and at this frequency the output is reduced by between 20 and 30 %. The variation occurs owing to individual residual strains in the "as grown" crystals without pumping. Experimental work therefore needs to be done to determine what further reduction occurs as the repetition rate is increased to 100 Hz.

Similar effects in the amplifier stages also cause the plane of polarization of an incident beam to be scrambled during amplification. In a worst-case analysis it may therefore well be that by the time the beam has traversed two amplifiers only 50 % of the output energy occurs in one polarization direction.

Depolarization in the amplifier stage is only critical in 90° scattering, but not in forward scattering.

JK-Lasers has a contract with IPP to deliver a YAG laser system providing 1 J in a single polarization at a repetition rate of 100 Hz (minimum 50 Hz) for at least a 1 second period. This laser has been ordered for quasistationary 90° scattering experiments in ASDEX. The time scale is estimated to be about 9 months from now. The laser will consist of a YAG oscillator followed by a series of amplifiers. JK-Lasers already produces standard systems of this type which have yielded up to 500 mJ per pulse at 50 Hz (unpolarized) on a continuous duty basis. This system consists of an oscillator followed by one amplifier. Consequently, if one considers this approach to achieve the required specification, allowance has to be made for the provision of at least one further amplification stage. The exact number of amplifiers required to achieve the full 1 J specification in a single polarization will be determined during the contract. The use of more than one amplifier adds the problem of interactions between them, and consequently provision has to be made for Faraday isolators between the amplifier stages to prevent self-oscillation. The experience gained in this development work will be available for JET.

2. Nd-glass laser

The alternative laser material which also operates at around 1.06 μm is Nd-glass. Nd-glass has a significantly lower gain coefficient than Nd-YAG, and consequently it is easily possible to obtain more than 1 J in a Q-switched pulse from a single glass oscillator. However, owing to the poor thermal and mechanical properties of glass, such lasers are generally operated at relatively low average output powers (typically below 10 W). However, the requirement here is not for continuous high output powers, but merely for a period of some seconds. It is therefore worthwhile to consider the total input energy required to achieve 100 to 1000 Q-switched pulses from a glass oscillator. This would appear to be in the region of a total of 50 000 J, and with a 10 minute inter-burst period it is believed that such an input

would not lead to thermal fracture of the laser rod. Two further problems might be expected with such a Nd-glass system. The first is the effect of pump-induced strain birefringence, which is even worse in the case of glass, and it might therefore be expected that the Q-switched pulse energy will rapidly fall as the number of pulses builds up in the burst. The second problem expected is due to the thermal lensing occurring when laser rods are excited, which with the conventional silicate-based glass laser rods would lead to extremely high laser beam divergence with the possibility of the resonator becoming completely unstable. However, the possibility now exists of using an athermalized glass recently developed for the high-energy laser programmes. Two sources of supply are available for this material, which is based on a phosphate glass which moves the laser operating wavelength to 1.054 μm: either Hoya (type LGH8) or Owens-Illinois (type EV4).

In these materials the variation of the refractive index with temperature is negative, and this almost exactly compensates for the change in optical length of the laser rod due to its expansion coefficient. This property in the case of EV4 glass leads to the definition of a thermal optic coefficient which is a factor of at least 15 smaller than for the conventional ED2 silicate glass. For a brief period it should thus be possible to run the glass at an average output power of 100 W with only the same lensing effect that would occur with the silicate laser rod running at an average power of between 6 and 8 W. The practical problem in running such tests is centred around the provision of a suitable power supply. It is proposed that a 9" x 3/8" rod should be used in a fourlamp pumping chamber, which is a standard J K Lasers glass amplifier rod configuration. This configuration has been regularly used with input pulse energies of a few thousand J in a time scale of 500 μs. It is proposed by J K Lasers that each lamp should be fed from a single 100 μF capacitor operating in the region of 1 kV. The capacitors would be isolated from the simmered lamps by individual thyristors. Each capacitor would then be resonantly charged in a time of approcimately 6 ms from a variable voltage high-power DC bank. This is the same

technique used in the standard J K Lasers 50 Hz YAG systems and only requires an increase in the average power capability.

The complete glass system would therefore consist of a single laser oscillator head and one large power supply. It would occupy the minimum space and be the simplest device to operate. The proposed time scale for determining the feasibility of this scheme is estimated to be between 4 and 6 months within a development contract. A further 2 to 3 months would then be required to engineer a system suitable for delivery.

3. Exciplex laser

Since their first realization in 1976 discharge-pumped rare-gas-halogen exciplex lasers e.g. KrF, XeF, have been brought to a rather high standard. The most important emission lines are ArF (1930 Å), KrF (248O Å), XeF (3500 Å) and XeCL (3080 Å). These lasers have a great potential for high average power applications. A high-velocity gas circulation allows repetition rates of more than 100 Hz,which lead to average output powers of up to 10 W in the UV in the present state of the art . The pulse widths of these gain-switched lasers are about 15 ns. The shortest wavelength line for scattering applications is 248 nm (KrF) because quartz can still be used for optics and windows and the detection of the scattered light can still be done by multipliers with high quantum efficiency.

At the moment the available energy per pulse is typically 200 mJ at 10 Hz and 100 mJ at 100 Hz, which is not sufficient for scattering experiments in JET. There are, however, several developments to increase this energy to about 1 J/pulse at more than 100 Hz, e.g. at Λ-Physics in Göttingen (West Germany).

4. Other lasers

The other lasers in our tables are far from being suitable for scattering applications

where high average power in a repetition mode is required: ruby because of poor thermal behaviour, dye lasers because of their long pulse duration, Cu vapour because of the too small single pulse energy.

5. Summary

At present YAG technology is the most developed, whereas in the field of exciplex lasers considerable improvements can be expected. The decision in favour of one of these two laser systems should be taken when the first experience with the Nd-YAG laser for ASDEX is obtained. This will be the case in the second half of 1980. In the following, we shall elaborate a scattering experiment with a Nd-YAG laser.

C) Technical problems

I. Layout of a forward scattering experiment

In this arrangement the laser beam is passed tangentially through the torus in the equatorial plane. Figure 2 shows a top and a side view of the beam paths inside the torus.

In order to avoid very small scattering angles, which would entail stray light problems, the plane of k-vectors is chosen to be the vertical one. A scattering volume at the centre of the plasma can then be observed at a maximum angle of 9°. It can be shown (see Appendix 1) that $\pm 1^{\circ}$ is allowed because otherwise spectra of considerably different half-widths would be superposed on each other, thus complicating interpretation. A scattering angle of $8^{\circ} \pm 1^{\circ}$ is therefore chosen.

The whole solid angle of this hollow cone, however, cannot be used since the window ports vignette most of it. Only two beams with a horizontal aperture of 6° each can

therefore be used.

The setup shown in Fig. 5 is proposed for implementing the forward scattering experiment. The concept of this setup is to couple mechanically the collection optics with the beam focusing optics. The arrangement is thus less sensitive to vibrations, and alignment is facilitated. However, for the forward scattering scheme one has to tackle the problem that at least one additional reflector is necessary, thus introducing a further optical element that can move independently. It will, however, become evident that the alignment becomes easy by the mechanical coupling mentioned, and that remote control of the optical elements is possible.

There is a rigid platform outside the radiation shielding wall which supports both the laser and the spectrometer plus detection system. The emitted laser beam will be parallel to the optical axis of the transmission optics. After traversing the radiation shielding wall by means of two 90° deflecting mirrors the laser beam is focused into the torus by lens L3 (Fig. 5). This lens is mounted on a movable support, this facility allowing a radial scan of the plasma (discharge-to-discharge experiment). The diverging beam which leaves the torus through the opposite window port no. 7 is reflected back and focused again into the plasma in the focal plane of lens L3.

There are several possible solutions for the problem of returning and refocusing the laser beam:

1) The beam can be collimated by a lens and then returned by
   a) a cat's eye retroreflector
   b) a corner cube retroreflector or
      a triple mirror retroreflector

   and
   c) an array of corner cube retroreflectors.

The use of a cat's eye retroreflector is inhibited by the too high laser intensity at the mirror surface. The commercial availibility of a single large ($\sim$ 220 mm dia.) corner cube or triple mirror retroreflector of the required accuracy ($< 1''$) will be investigated. Corner cube arrays of this accuracy are readily available.

2) The beam can be returned and refocused by a single spherical mirror.

Solution 1) requires no mechanical stability, but high quality of the optical components. In contrast, solution 2) transfers all requirements on to the mechanical alignment.

There are intermediate solutions which distribute the requirements between mechanical and optical components (e.g. an inverted beam expander followed by a retroreflector, whose necessary precision is less since the beam divergence is higher whereas simultaneously its size can be much less).

The most favourable solution for the reflector (up to now described as mirror M1) would be to use a corner cube retroreflector rigidly coupled with a lens. In this case the focal spots of the incoming laser beam (formed by lens L3) and that of the reflected laser beam are identical. This solution would be very stable since vibrations of the support no. 2 (Fig. 5) would not influence the experiment (maladjustment of the distance between support No. 1 and support No. 2 is uncritical owing to the very long beam waists).

However, when a corner cube is used laser radiation is coupled back into the laser, this being a problem when there are amplifier stages (prelasing!). Isolation by means of polarization techniques is not feasible if an unpolarized laser beam is used in this forward scattering experiment. But it is supposed that the long optical path to the retroreflector will reduce the feedback. The use of an active shutter in front of the

laser as well as the possibility of decoupling by means of a bleachable dye cell should be investigated in a test setup using the very same laser and identical optics as used in the scattering arrangement.

If it turns out that feedback is harmful to the laser and cannot be avoided, we shall consider as a second solution an arrangement in which the focal volumes of the incoming and reflected laser beams do not overlap. For this purpose a spherical mirror M1 is used as reflecting and focusing element and its optical axis is deliberately misaligned. Since this adjustment is sensitive to tilting of the mirror, either a feedback control of the adjustment is necessary during laser operation (described in Sec. C VIII), or an effective isolation against vibrations must be used.

A parabolic mirror M2 collimates the scattered light from the focal volume. There are two collection optics possible, one on top of the laser beam and one below. We shall only use one of them but the other will remain optional (use of a second spectrometer and detection system in order to increase the dynamic range of the measurements). Mirror M2 is used off axis as shown in more detail in fig. 6. The plane mirror M3 then directs the collimated beam parallel to the incoming laser beam towards the detection system. The two mirrors M2 and M3 as well as lens L3 are mounted in a rigid frame and are adjusted relative to each other before the frame is inserted into the optical setup.

II. Collection optics

Besides the necessary window (see fig. 5) the optical components of the collection optics within the torus hall are reflectors. With the required achromatism, this solution is favourable in the case of high radiation fluxes. For the mentioned window the use of either quartz or of γ -radiation -resistant (highly cerium-stabilized) glass type SCHOTT BK 7 G 25 is proposed. This glass type only shows minor increase in

absorption in the short wavelength region of the visible spectrum after being irradiated with high doses of energetic gamma radiation. The effect of neutrons has to be evaluated in a test experiment. A comparison between quartz and cerium-stabilized glass must be performed.

A side view of the collection optics and the lens L3 as mounted in the rigid frame is given in fig. 6. M2 is a parabolic mirror with a focal length of f = 5000 mm and an aperture A = f/9.5. It will be used off axis at an angle of $\alpha = 7.5^{\circ}$. In that case the coma blur diameter and the astigmatism blur diameter according to

$$\text{Coma } \phi \approx \frac{\alpha}{16} \frac{A^2}{f} \qquad (4)$$

α in [rad]

$$\text{Astigmatism } \phi \approx \frac{\alpha^2}{2} A \qquad (5)$$

are 0.5 mm and 5 mm respectively. Since we want to image a focal spot diameter of 10 mm, these values are tolerable and no expensive off-axis paraboloid is needed.

Figure 7 shows a cross-section of the beams in the plane of mirror M2. This mirror will be cut out in order to let the beam returning from mirror M3 pass. The radiation shielding wall will be traversed using two mirrors as shown in fig. 5.

A parabolic mirror M4 mounted on the common platform for the laser and detection system will image the scattering volume onto the entrance slit of the spectrometer (see fig. 8). The cross-section of the entrance slit and the magnification of the collection optics define the cross-section of the observation beam in the focal plane of the laser.

III. Transmission losses

The transmission losses of the laser beam up to the scattering volume are summarized

in Table V, whereas those for the scattered light are listed in Table VI.

Table V

Element	No. of passes	Transmission
Beam expander, Schott BK 7, AR-coated	1	0.9
$2 \times 90^{\circ}$ deflection mirrors	1	$(0.95)^2$
f = 4 m focusing lens Schott BK 7 G 25 (cer. stab.) uncoated	1	0.9
Port window Schott BK 7 G 25 (cer. stab.) uncoated	1	0.9
Port window Schott BK 7 G 25 uncoated	2	$(0.9)^2$
f = 5 m focusing mirror	1	0.95
	overall transmission	0.51

Table VI

Element	No.of passes	Transmission
Window port Schott BK 7 G 25 uncoated	1	0.9
2 off axis collection mirrors	1	$(0.95)^2$
2 x 90° deflection mirrors	1	$(0.95)^2$
Focusing mirror	1	0.95
Collimating mirror	1	0.95
Grating	1	0.7
Imaging mirror	1	0.95
Relay lens, Ar-coated	1	0.9
	overall transmission	0.39
+ Notch filter (Interference filter)	1	0.5
	overall transmission	0.19

IV. Spectrometer

The requirements for a grating spectrometer applicable to the proposed scattering experiment are fixed by the étendue of the scattered light and the minimum channel width. From the following equations the dimensions of the spectrometer must be calculated:

1. $$d_1 \frac{\Phi_{M5}}{f_{M5}} = \Delta x \frac{\Phi_{M2}}{f_{M2}} = const \qquad (6)$$ (conservation of étendue)

2. $$D = \frac{\Phi_{M5}}{\cos \alpha} \qquad (7)$$

3. $$\frac{dx}{d\lambda} = \frac{m f_{M6}}{c \cos \beta} \qquad (8)$$

4. $$d_2 = \Delta\lambda \frac{dx}{d\lambda} \qquad (9)$$

Thereby

d_1 = width of entrance slit

d_2 = minimum width of exit slit

Δx = width of the scattering volume

Φ_{M5} = diameter of collimating optics

Φ_{M2} = diameter of observation mirror M2

f_{M5} = focal length of collimating optics

f_{M6} = focal length of focusing optics

f_{M2} = focal length of the observation mirror M2

D = length of the ruled area of the grating

α = angle of incidence

β = angle of diffraction

$\frac{dx}{d\lambda}$ = linear dispersion in the focal plane

$\Delta\lambda$ = bandwidth of the narrowest spectral channel

c = grating spacing

m = order of diffraction

Assuming $f_{M5} = f_{M6}$, $\cos\alpha \approx \cos\beta$ and $m = 1$ the relation

$$D = \Delta x \cdot \frac{\Phi_{M2}}{f_{M2}} \cdot \frac{c}{\Delta\lambda} \qquad (10)$$

results for the dimension of the ruled area of the grating.

The required minimum spectral width of a channel for optimum detection (see C VII) in the low temperature region is $\Delta\lambda = 40$ Å.

The value of $\Delta x \cdot \frac{\Phi_{M2}}{f_{M2}}$ is given by the experimental layout to be $\Delta x \cdot \frac{\Phi_{M2}}{f_{M2}}$ = 1,05 mm (Δx = 10 mm, $\frac{\Phi_{M2}}{f_{M2}} = 1/9.5$).

A reasonable grating blazed at $\sim$ 1 µm has a value of $c = \frac{1}{1200}$ mm. Thus a length of the ruled area D = 220 mm is required. This requirement can be met approximately. Bausch and Lomb supplies standard plane reflectance gratings with lengths of the ruled area of up to 206 mm and a groove length of 154 mm.

A possible solution of a grating polychromator would make use of a Bausch and Lomb grating 35 - 53 - 28 - 530 (1200 grooves/mm, blaze angle 36° 52′ for a wavelength of 1 µm in Littrow mounting), two parabolic mirrors used off axis with a focal length $f_{M5} = f_{M6} \approx 1.7$ m, a diameter $\Phi_{M5} \approx 230$ mm, an entrance slit of 10 x 20 mm^2 and an array of special cut lenses located in the focal plane. The lenses shown in fig. 9 concentrate the radiation onto the active areas of the detectors. The optimum distribution of channel widths is discussed in Sec. C VII.

For convenience a summary of all values of the spectrometer is listed:

d_1	= 10 mm	f_{M5}	= 1700 mm	$\frac{dx}{d\lambda}$	= 0.255 $\frac{mm}{\text{Å}}$
d_2	= 10 mm	f_{M6}	= 1700 mm	$\Delta\lambda$	= 40 Å
Δx	= 10 mm	f_{M2}	= 5000 mm	d	= $\frac{1}{1200}$ mm
Φ_{M5}	= 230 mm	D	= 220 mm	m	= 1
Φ_{M2}	= 525 mm	$\alpha \approx \beta$	$\approx 37^\circ$		

In addition, a series of interference filters may be inserted in front of the detectors in order ot suppress laser stray ligth and higher orders of short wavelength plasma radiation.

In the course of preparing the periodically pulsed scattering experiment for ASDEX, the alternative solution of using interference filters only will be discussed and compared with the grating spectrometer.

V. Detectors

The detection system consists of an array of silicon avalanche photodiodes of large active area (3 mm Ø), model General Electric 50 EHS (see data sheet no. 1). The étendue of these detectors is sufficiently high that all scattered light collected can be accepted. These detectors feature a high quantum efficiency at the laser wavelength.

Since the noise mechanism of these detectors is important for the subsequent signal - to - noise considerations they will now be briefly described. The dark current I_d as given in the data sheet consists of two parts /3/:

a) a component I_{db}, which experiences the avalanche amplification (gain factor M) and

b) a component I_{ds} (leakage current at the guard ring), which is not amplified.

One thus has

$$I_d = I_{ds} + MI_{db}. \qquad (11)$$

Typical values for silicon avalanche photodiodes are

$I_{ds}' \approx 3 \times 10^{-8}$ A/mm circumference of the active area
$I_{ds} \approx 2.8 \times 10^{-7}$ A for 3 mm Ø
$I_{db}' \approx 10^{-10}$ A/mm^2 active area.
$I_{db} \approx 7.1 \times 10^{-10}$ A for 3 mm Ø .

The quantity of interest for the S/N considerations is not the DC part of the dark current but the mean square noise current $\langle \delta I_d^2 \rangle$ given by /3/:

$$\langle \delta I_d^2 \rangle = \left[I_{ds} + I_{db} \cdot M^2 \cdot F(M) \right] 2qB \qquad (12)$$
$$= (2.8 \times 10^{-7} \text{ A} + 7.1 \times 10^{-10} \text{ A} \times 10^4 \cdot F) \cdot 2qB \quad \text{for 3 mm Ø, } M = 100$$

q = elementary charge; B = bandwidth; F = excess noise factor.

From this relation it becomes evident that the important contribution to the dark current noise stems from the amplified bulk current component: $\langle \delta I_d^2 \rangle \approx I_{db} M^2 \cdot F(M) \cdot 2qB$ (12 a). Furthermore the appearence of the factor F(M), the excess noise factor defined as

$$F(M) = \langle M^2 \rangle / \langle M \rangle^2, \qquad (13)$$

shows that the amplification is not noise-free and must be taken into account for the signal - to - noise calculations.

I_{ds} and I_{db} are not specified separately in the data sheet no. 1 but can be determined when the dark current is measured as a function of the gain. Measured values for the specimen JJW (data sheet no. 2) are

$I_{db} = 3.5 \times 10^{-10}$ A
$I_{ds} = 4.5 \times 10^{-8}$ A at 20° C.

The excess noise factor for this specimen was determined to be F = 10 at 20°C (M = 100).

Amplification of the small amplitude avalanche-photodiode output signals is achieved using low-noise impedance transformers with FET transistors. The bandwidth of the system corresponds to a gate time of 50 ns. The noise of the impedance transformers is low enough to be neglected in the SNR calculations.

VI. Signal-to-Noise ratio

The problem of signal- to - noise ratio for single shot laser scattering experiments has been treated e.g. by /4,5/. This treatment does not consider effects occurring when the internal amplification within the detector is not free of noise, a simplification which is justified for the case of the commonly used photomuliplier. However, when avalanche photodiodes are used these effects cannot be neglected. In order to evaluate their influence we use the SNR treatment for avalanche photodiodes as given by /3/.

A signal modulated at a centre frequency ω is incident on the avalanche photodiode (see fig. 10).

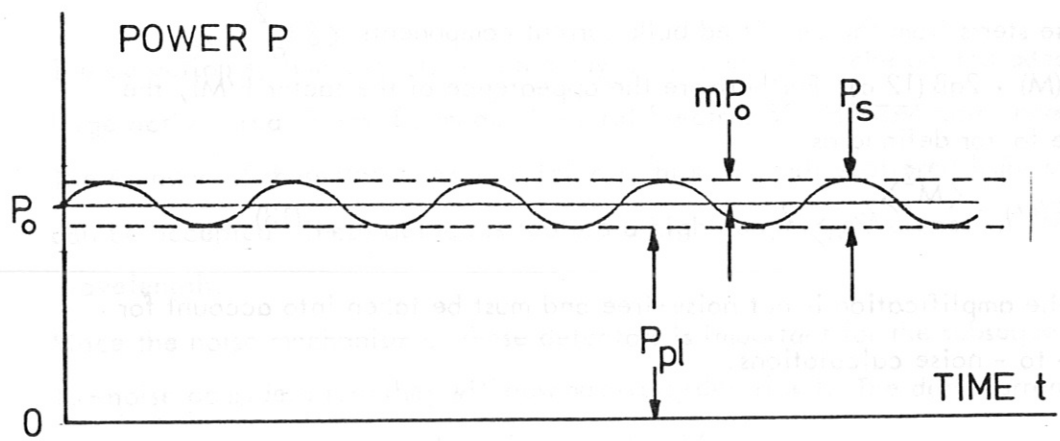

Fig. 10: Radiation power incident on the detector.

The signal is detected within a narrow bandwidth B. For this situation the time-averaged signal - to - noise ratio (e.g. see /6/) is written as

$$\left\langle \frac{S}{N} \right\rangle_t = \sqrt{\frac{(P_o m R_o M)^2/2}{2q[I_{ds} + (P_o R_o F_s + I_{db} F_d) M^2] B + i_{na}^2}} \qquad (14)$$

where P_o = average intensity of light incident on the detector

m = modulation depth

R_o = unity gain responsivity = $\frac{q\eta}{h\nu}$ (η = quantum efficiency)

M = gain

q = elementary charge

B = bandwidth

I_{ds} = dark current component undergoing no amplification (will be neglected compared with $I_{db} \cdot M^2 \cdot F$ due to equation (12 a))

I_{db} = dark current component undergoing amplification

i_{na}^2 = equivalent mean square noise current of the subsequent amplifier, neglected in the following. This neglect is justified for the radiation power levels in the forward scattering experiment considered.

F_s, F_d = excess noise factor = $\langle M_{s,d}^2 \rangle / \langle M_{s,d} \rangle^2$ for the signal and the amplified component of the dark current respectively. For our estimations of S/N-ratios $F_s \approx F_d \approx F$.

Firstly this relation can be rewritten neglecting I_{ds} and i_{na}^2 and introducing the noise equivalent power NEP defined by

$$NEP^2 R_o^2 M^2 B = \langle \delta I_d^2 \rangle \approx I_{db} M^2 F \cdot 2qB \qquad (15)$$

to yield

$$\left\langle \frac{S}{N} \right\rangle_t = \frac{P_o \cdot m}{\sqrt{2 \cdot \frac{B}{R_o} \cdot (NEP^2 R_o + 2q P_o F)}} \qquad (16)$$

Secondly, we separate the incident light power in fig. 10 into a component P_{pl}, representing the plasma radiation and a component P_s, representing the scattered light.

$$m P_o = \frac{P_s}{2} \qquad (17)$$

$$P_o = P_{pl} + \frac{P_s}{2} \qquad (18)$$

Replacing in addition the unity gain responsivity R_o by $q\eta/h\nu$ we obtain

$$\left\langle \frac{S}{N} \right\rangle_t = \frac{P_s}{\sqrt{\frac{F\,h\nu}{\eta}} \sqrt{8B\left(\frac{NEP^2\,\eta}{F\,h\nu} + 2P_{Pl} + P_s\right)}} \qquad (19)$$

Inserting $B = \frac{1}{2\tau}$ (τ represents the half-width of the scattered pulse) yields the relation

$$\left\langle \frac{S}{N} \right\rangle_t = \frac{P_s}{\sqrt{\frac{F\,h\nu}{\eta\,\tau}} \sqrt{4\left[P_s + 2\left(P_{Pl} + \frac{NEP^2\,\eta}{2\,h\nu\,F}\right)\right]}} \qquad (20)$$

This relation shows the same structure as the equation commonly used for scattering experiments when excess noise mechanism for the amplification process can be neglected:

$$\frac{S}{N} = \frac{P_s}{\sqrt{\frac{h\nu}{\eta\,\tau}} \sqrt{P_s + 2\left(P_{Pl} + \frac{NEP^2\,\eta}{2\,h\nu}\right)}} \qquad (21)$$

By comparison the effect of the excess noise resulting from amplification becomes evident: The effective quantum efficiency is reduced by the excess noise factor F. Thus the well-known equation (21) can be used simply by replacing the quantum efficiency η by the effective quantum efficiency η/F.

The relation obtained can also be formulated in terms of photons n_s and n_{pl}, the quantum numbers of scattered and plasma light, respectively;

$$\frac{S}{N} = \frac{n_s}{\sqrt{\frac{F}{\eta}\left[n_s + 2\left(n_{PL} + \frac{n_D}{F}\right)\right]}} \qquad (22)$$

$$n_D = \frac{NEP^2 \cdot \eta \cdot \tau}{2(h\nu)^2} \qquad (23)$$

For two representative sets of parameters (same plasma parameters, two different laser energies) numerical values are given inTable VII. For this evaluation the detector data (NEP = $1{,}5 \times 10^{-13}$ $W/\sqrt{Hz}$, F = 10 for M = 100) measured at room temperature were used.

The numbers for photons and $n_{D/F}$ given in Table VII show that for the given parameters $n_{D/F}$ is small compared with n_s and n_{pl}. In this case the NEP of the detector can be neglected and the S/N is proportional to $1/\sqrt{F}$. This indicates the possibility of improving the S/N by reducing the gain and thus the excess noise, a method discussed in /7/. For instance at romm temperature and gain M = 25 a value F = 5 was measured. The corresponding S/N ratios for 1 and 0.3 J laser energy are 10.5 and 3.8 respectively. (see Table VII)

Table VII

Θ	$= 8^{\circ}$	
n_e	$= 1 \times 10^{13}\ cm^{-3}$	
T_e	$= 4$ keV	
K	$= 100$	
τ	$= 50$ ns	
d	$= 1$ cm	
l	$= 14.5$ cm	
	$\hat{=}$ 20 mm spectrometer slit height	
V_{pl}	$= 2 \times 1 \times 800\ cm^3$	
$\Delta\Omega$	$= 8 \times 10^{-3}\ sr$	
$T_{coll.opt.}$	$= 0.1$	
$\varepsilon_{pl}\ (\lambda = 1\mu m)$	$= 1.1 \times 10^{-12}$	$\frac{W}{\text{Å}\ cm^3\ sr}$
$\Delta\lambda$	$= 1/6\ \Delta\lambda$ FWHM	see Sec . B II b
$E_{s,\Delta\lambda}$	$= E_s/12$	see Sec . B II b

$E_L = 1$ J	$E_L = 0.3$ J
$n_s = 4100$	$n_s = 1230$
$n_{pl} = 1940$	$n_{pl} = 1940$
$n_{D/F} = 483$	$n_{D/F} = 483$
S/N = 7.5 (M = 100, F = 10)	S/N = 2.7 (M = 100, F = 10)
S/N = 10.5 (M = 25, F = 5)	S/N = 3.8 (M = 25, F = 5)

There also remain to be investigated in detail possible improvements by changing the operating temperature of the photodiodes. These measurements are currently being performed in the course of preparing the 90° scattering experiment for ASDEX.

The improvements in the S/N values which seem feasible offer the possibility to increase the spatial resolution of the measurements by reducing the slit height of the polychromator (see fig. 3 and Sec. C. XII). This is of course also possible for electron densities above 1×10^{13} cm^{-3}, where reduction of the gain is possible.

VII. Optimum channel distribution

The problem is how to distribute the spectral channels in order to get both high dynamic range in the electron temperature measurements and simultaneously the smallest possible errors.

Different types of channel distributions symmetric to the laser wavelength have been investigated, equidistant ones and those where the channel width decreases towards the centre of the spectrum.

In the model computations first the signal amplitudes and the signal - to - noise ratios of the different channels of an assumed channel distribution are calculated. Relativistic effects in the spectrum are neglected (see Appendix 2). The energy of the laser pulse at the scattering volume is taken as 1 J unpolarized. Furthermore $\Theta = 8°$, $\Delta\Omega = 8 \times 10^{-3}$ sr, a length of the scattering volume of $l = 14$ cm (corresponding to a slit height of the spectrometer of 20 mm), an electron density of 10^{13} cm^{-3} and a transmission of the collection optics of 0.1 are assumed. Concerning the plasma background radiation, $K = 100$ is chosen. The radiating plasma volume

is $1 \times 2.0 \times 800\ cm^3$. The gating time is 50 ns. With regard to the noise properties of the avalanche photodiode and the amplifier the pessimistic values for room temperature given in Sec. CV are used.

Secondly, a Gaussian profile is fitted numerically to the signals, which are weighted with their S/N values. Thus the temperature and the relative errors are determined.

In fig. 11 the error in electron temperature is given as a function of the electron temperature for different sets of equidistant channels omitting the centre (broken lines). To demonstrate the advantage to be gained with respect to the dynamic range of the measurement an example is given, too, for a case where the channel width decreases towards the centre of the spectrum (solid line).

From fig. 12 it becomes evident that more than approx. 2 x 5 optimal distributed channels will give only little improvement in the dynamic range.

VIII. Alignment procedure

The alignment procedure is described for the more complicated case using a spherical mirror M1 instead of a retroreflector.

The alignment has to be done in the following steps:

1) The windows W 1, W 2 and W 3 are tested to show a wedge of less than 1'.

2) The focusing lens L 3, the collimating mirror M2 and the beam steering mirror M 3 are aligned within the rigid frame so that the foci are separated by Δ y (see fig. 8) using two laser beams parallel to each other and parallel to optical axis of L_3. The distance Δ y is chosen to be somewhat larger than the focal spot diameter of the Nd-laser beam (~ 3.5 mm). A value of Δ y $\approx$ 10 mm is sufficient. Then the optical elements are fixed with respect to the frame . This alignment may be done outside the experimental hall.

   The plane reflecting mirror M 7 is fixed to the frame perpendicular to the

optical axis of lens L 3 within the required accuracy of ≈ 0.5 mrad.

The rigid frame stands on three supports which fit into three corresponding bearings on a platform mounted upon support no. 1. This platform can be remote adjusted with respect to the y and x coordinates vertically to the optical axis of the laser beam and also with respect to the angles α and β in the horizontal and vertical planes. The z-position is controlled by the movement of the support along the rails.

3) The rear frame containing the focusing mirror M1 is attached to the support no. 2 in a manner similar to that described in 2). The supporting platform can be controlled remotely with respect ot the angles α and β .

4) The beam steering mirrors M8 and M 9 within the port of the radiation shielding wall are mounted in a rigid frame and adjusted for parallel beam displacement.

5) The neodymium laser, the beam expander and the grating polychromator together with the imaging mirror M 4 are mounted on the very same rigid structure. Alignment is performed with the help of a 1.15 μ He-Ne laser beam injected from the image plane of the polychromator in such a way that the optical axis of the detection optics is parallel to the expanded Nd-laser beam.

6) Two He-Ne laser beams (6328 Å) are injected into the Nd beam optics, as shown in fig. 8. These beams are used to monitor any tilting of the rigid frame for L 3, M 2 and M 3 as well as the relative movement of this frame with respect to the focusing mirror M 1. It can be shown (see Appendix 3) that the chromatic differences in focal lengths of the optical elements can be neglected within the required accuracy.

7) The rigid platform supporting the laser and detection optics is now adjusted so that

the neodymium laser passes through the tokamak vessel (rigid fram with L 3, M 2 and M 3 as well as mirror M 1 removed).

8) The rigid frame is put into place. Adjustment is such that the He-Ne beam is returned collinear by mirror M 7. (This establishes α and β of the frame.) Adjustment of x and y is such that the neodymium beam passes the vessel without being vignetted. The place where the He-Ne beam hits mirror M 7 will then be marked. The z-position of the frame is easily adjusted to the required accuracy, which is of the order of 1 cm.

9) Mirror M 1 is put into place. The x and y positions are adjusted so as to centre the mirror with respect to the optical axis. Then the mirror is tilted (α and β) to let the returning He-Ne beam pass the plane of the pinhole of the beam expander at a distance $\Delta y \cdot \frac{f_{L2}}{f_{L3}}$ from the axis (typical value: 6mm). Check that the returning Nd-beam coincides with the returning He-Ne beam at that place.

At this plane the He-Ne beam and the neodymium beam are separated by a dichroic mirror. A detector array will continuously monitor the position of the He-Ne spot, whereas the energy of the neodymium laser pulse is monitored with a calorimeter. (This monitor for the returning energy may indicate whether the windows become absorbing.)

Adjustment having been performed, we have to consider movements of the different parts of the setup during operation of JET:

1) The JET vessel moves (relative to the laser platform).

As long as the vertical movement does not exceed 100 mm, no vignetting of the

laser beam and the collection beam occurs. Since windows are plane-parallel, no beam deviation occurs.

2) The rigid frame containing L 3, M 2 and M3 moves.

a) Movement along the z-axis is uncritical (upper limit $\approx$ 3cm).

b) Movement in the plane perpendicular to the optical axis is tolerable up to amplitudes of $\approx$ 1 cm and can be monitored separately.

c) Tilting can be corrected by computer control (adjustment is checked continuously by He-Ne laser).

3) The reflector M 1 moves.

In the event that the corner cube reflector can be used any movement is uncritical. In case the spherical mirror has to be used, tilting has the same effect as a translation. Any movements are measured continuously with the help of the He-Ne-beam and the rigid frame for M 1, is tilted to cancel them out.

It is highly probable that the mentioned automatic adjustment of the rigid frame (with L 3, M 2, M 3) during the JET discharge is not necessary and that the alignment will only be checked between the discharges. The supports no. 1 and 2 as well as the rigid frame and the mirror mount should preferably be made from dielectric material to avoid vibrations due to eddy currents.

IX. Calibration

The calibration of the channels relative to each other will be performed using a black-body radiator. The stability of this calibration will be checked continuously throughout the measurements using a pulsed light emitting diode (e.g. Plessey GAL 102 F). The emitted spectrum of this diode is 600 Å wide and thus covers the whole range of spectral channels. This radiation will be injected via light guides at the entrance slit of the spectrometer.

The LED will be pulsed between the neodymium laser pulses. Besides checking the calibration the signals from the detectors will also be used for setting the computer controlled gain of the avalanche photodiodes (via the applied voltage).
It should be noted that this continuous control of the gain is only necessary when the avalanche photodiodes are operated at high gain, where the gain depends critically upon temperature and voltage. This is an additional argument to operate the diodes at lower gain (discussed in Sec. C VI).

The absolute calibration for the measurement of the electron density will be performed on the basis of the single pulse ruby scattering diagnostics.

X. Data acquistion

For the case of a fast detector the typical signal to be recorded is shown in fig. 13.

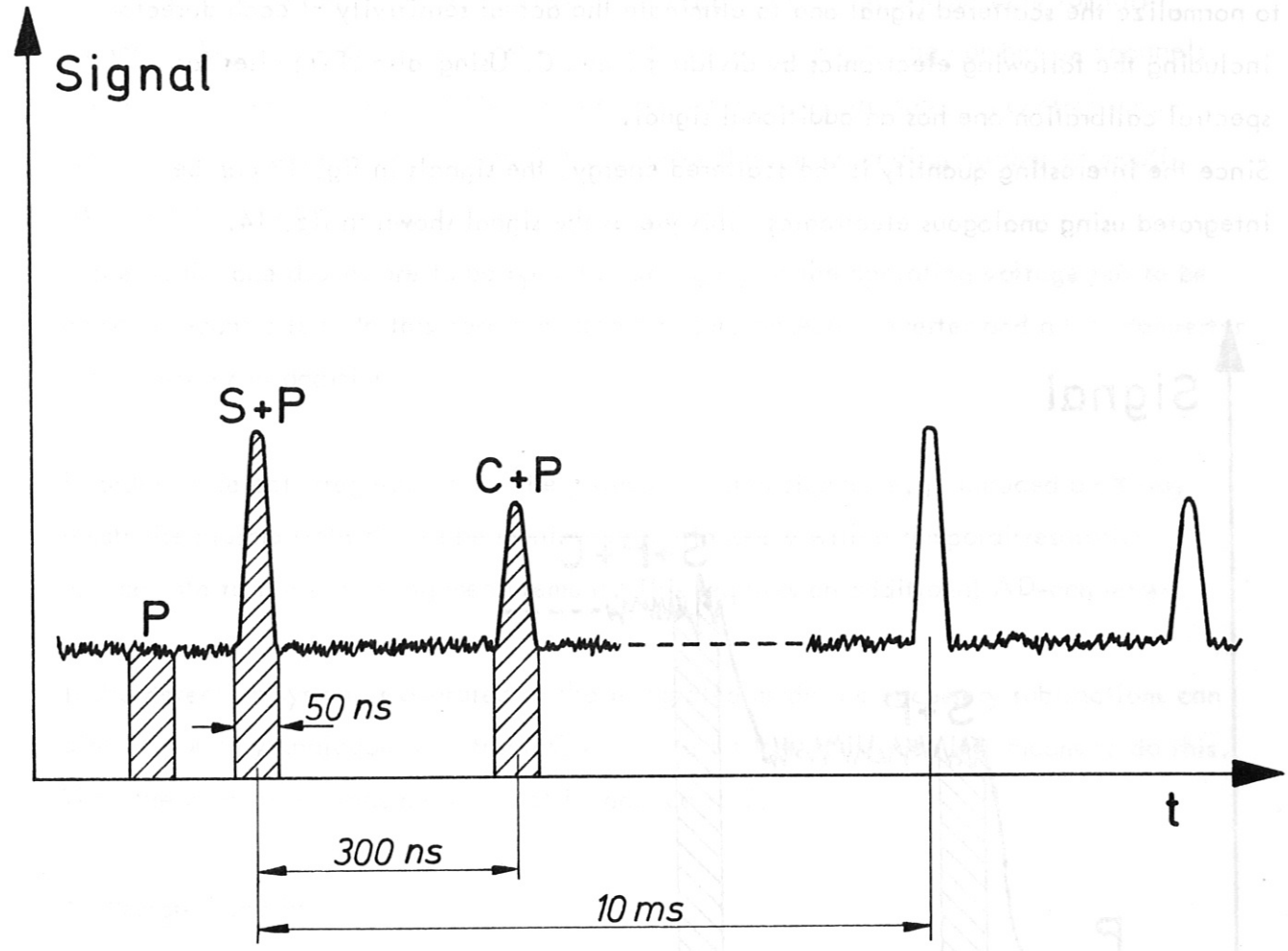

Fig. 13: Typical signal obtained with a fast detector (P = plasma radiation; S = scattered radiation; C = calibration pulse. The gates are indicated by hatching.)

For the calibration pulse C preferably the delayed laser pulse is used. This pulse serves to normalize the scattered signal and to eliminate the actual sensitivity of each detector including the following electronics by dividing S and C. Using also LED pulses for spectral calibration one has an additional signal.
Since the interesting quantity is the scattered energy, the signals in fig. 13 can be integrated using analogous electronics. This yields the signal shown in fig. 14.

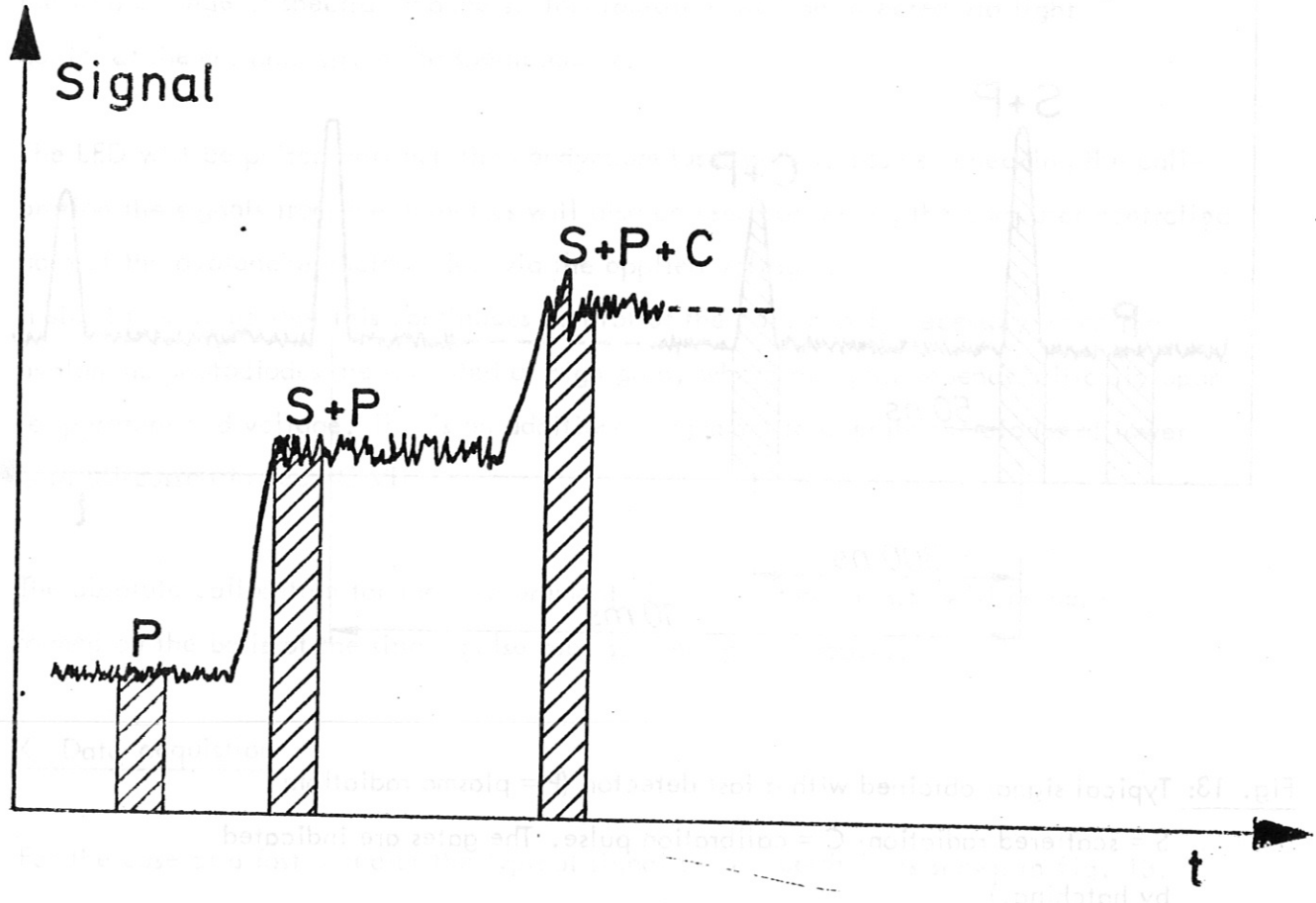

Fig. 14: Integrated signal

The shown sequences of signals occur periodically with 10 ms intervals. So during the JET discharge time of 10 sec one thousand pulse sequences must be recorded from each of the ten spectral channels.

In both cases (real time as well as integrated mode) 3 AD-converters (4 in the case with LED-signal + corresponding memory) are necessary for each spectral channel. There are AD-modules with 12 channels in development which are suitable for this purpose. These modules require fast memories with a corresponding number of channels. The whole system needs one CAMAC-crate and one crate controller. To control separately the input sensitivity of each AD-converter the corresponding number of amplifier modules is necessary.

If the avalanche diodes are to be operated at high gain the operating voltage has to be computer-controlled. In this case a microprocessor, an AD-converter and a DA-converter are necessary in addition.

In order to detect irregularities of the plasma emission signal, e.g. induced by X-ray bursts the plasma light should be monitored continuously with a temporal resolution appropriate to the scattering measurement. This requires an additional AD-converter.

If the detection system is operated in the integrated mode the necessary subtractions can also be done by analogous electronics. A matched filter is an adequate means to do this. Then the number of gates per channel is reduced to 2.

XI Remote handling

The set-up as described is suitable for remote handling.

There are some elements to be replaced from time to time owing to radiation damage namely:

1) The rigid frame with the lens L 3 and the mirrors M 2 and M 3 (prealigned);
2) the windows W 1, W 2, W 3;
3) the reflector M 1.

The windows will be constructed according to JET instructions so that they can be replaced using the manipulator.

The rigid frame as well as the reflector can be removed and replaced by the crane.

XII Applicability

a) Range of plasma parameters

The electron temperature range which can be measured within an error of $\approx$ 10 % will be

$$0.4 \text{ keV} \leqslant T_e \leqslant 12 \text{ keV}.$$

The electron density can be measured for

$$n_e \geqslant 1 \times 10^{13} \text{ cm}^{-3}.$$

The error of this measurement is about half as large as in the case of temperature measurement.

b) Spatial and temporal resolution

The laser beam passes tangentially through the torus. The resolution along the laser beam is constant ($l \approx 14$ cm). The corresponding resolution in radius is given in fig. 15. It is approximately 12 cm.
The duration of each single measurement is 50 ns, the repetition rate 100 Hz.

c) Accessible plasma region

The measurements are performed in the equatorial plane of the torus and provide a radial profile with $\approx$ 10 spatial points between the outer plasma boundary and the centre of the plasma (see fig. 15). Measurements at different spatial points will be performed by moving the optics between the JET discharges.

Appendix 1: Finite solid angle effects on the scattered spectrum

In the case of forward scattering the scattered spectra vary strongly with the scattering angle. The consequence of this effect on the evaluated temperature was investigated by summing up the contributions from the different scattering angles contained within finite solid angles (for a collecting optics with circular cross-section). The apparent temperature was then determined from the half-width of the spectrum obtained (for the centre scattering angle) and compared with the real value of the temperature. The result is shown in fig. 16. It can be inferred that for a tolerable error of the temperature of less than 10 % an angular spread of $\sim \pm 1^{\circ}$ is allowed for an 8° scattering experiment.

Appendix 2: Relativistic effects on the scattered spectrum

When taking into account relativistic effects (as necessary for temperatures above 1 keV)the spectra for 8° forward scattering are

a) much narrower,

b) much less shifted versus the blue, and

c) much more symmetric, Gaussian-like than those for the 90° case.

The effects 2 a and 2 b are illustrated by fig. 17 taken from Mattioli /8/.

Following the treatment of Mattioli we calculated for the 8° forward scattering the relativistic blue shift of the maximum and also the asymmetry of the spectrum. In fig. 18 the total half-width of the spectrum (composed of two parts, $\Delta\lambda_{red}$ and $\Delta\lambda_{blue}$, see fig. 19) normalized to the laser wavelength λ_L is plotted versus the scattering angle Θ .

In fig. 20 the asymmetry of the spectrum is given by plotting $(\Delta\lambda_{red} - \Delta\lambda_{blue})/(\Delta\lambda_{red} + \Delta\lambda_{blue})$ versus the scattering angle. Fig. 21 shows the relativistic blue shift of the maximum of the scattered spectrum as a function of the scattering angle.

It can be stated that:

1. From fig. 21 the blue shift of the maximum at 8° scattering angle is less than 3 % of the total half-width for temperatures of up to 10 keV.

2. Also the symmetry of the scattered spectrum will be conserved to within 5 % up to 10 keV (see fig. 20).

Owing to these statements it makes sense to investigate distributions of channels symmetric to the central wavelength in order to maximize the dynamic range of the temperature measurement.

Appendix 3: Alignment with a He-Ne laser, chromatic errors

The He-Ne laser (632.8 nm) is lined up with the neodymium laser beam as shown in fig. 8. Fig. 22 shows schematically the beam expanding telescope in order to discuss whether the two beams will be parallel within the required accuracy (given by the beam divergence of the expanded Nd laser beam). The He-Ne beam is injected at a distance h from the optical axis, and the mirrors M 11 and M 13 will be adjusted to pass the beams through the centre of the 2.2 mm Ø pinhole. This pinhole is located in the focal plane (for IR-radiation) of lens L 1.

The refractive indices of BK 7 glass at 1.014 μm and 643.8 nm are 1.50731 and 1.51472 respectively. Since the focal lengths of the lenses vary according to $f \propto (n-1)$, one has $f^{vis} = 0.9856\, f^{IR}$.

The He-Ne beams will pass the focal plane (for 632.8 nm) of lens L 2 in a distance ΔY from the optical axis:

$$\Delta Y = \alpha_0 \left(f_2^{IR} - f_2^{VIS} \right) = \frac{h}{f_1} \left(f_2^{IR} - f_2^{VIS} \right) \qquad (24)$$

This will lead to an inclination α_2 of the outgoing beams versus the optical axis

$$\alpha_2 = \frac{\Delta Y}{f_2} = \frac{h \left(f_2^{IR} - f_2^{VIS} \right)}{f_1 \cdot f_2} \qquad (25)$$

With h = 6 mm and f_1 = 400 mm, an angle α_2 = 0.22 mrad results, which is smaller than the beam divergence of the expanded neodymium laser beam (0.83 mrad) and is tolerable.

Concerning the overlap in the scattering volume of the He-Ne beam and the neodymium laser beam see fig. 23:

It is first assumed that the He-Ne-laser is parallel to the optical axis of lens L 3. The focal spot of the He-Ne-laser behind lens L 3 will then be 58 mm in front of the IR-focus. Thus the He-Ne beam will be $\Delta y = \beta (f_3^{iR} - f_3^{vis})$ from the axis in the focal plane of the neodymium laser beam. With $\beta = \frac{f_2}{f_1} \cdot h \cdot \frac{1}{f_3} = 10$ mrad a value $\Delta y = 0.6$ mm results.

Since the He-Ne-laser beam in reality is inclined against the optical axis by an angle of $\alpha_2 = 0.22$ mrad an additional displacement of 0.9 mm occurs. The total displacement of 1.5 mm is tolerable since the focal spot diameter of the 1.06 μm radiation is 3.5 mm.

Acknowledgement

We wish to thank Dr. E. Holzhauer, IPF, Stuttgart, for performing the measurements of NEP and excess noise of the avalanche photodiodes.

References

/1/ S. Glasstone, R.-H. Loveberg: "Controlled Thermonuclear Reactions", van Nostrand-Reinhold, Princeton, N.J., 1960

/2/ A. Eberhagen, W. Lünow: "Tabellen zur Auswertung von Intensitätsmessungen an Wasserstoffplasmen", Reports IPP 1/23, IPP 6/20 (64)

/3/ P.P. Webb, R.J. McIntyre, J. Conradi: "Properties of Avalance Photodiodes", RCA Rev. 35, 234 (74)

/4/ J. Lassalle, P. Platz: "Signal-to-noise Scaling of Ruby Laser Scattering from Large-Tokamak Plasmas", Plasma Physics 20, 107 (78)

/5/ H.F. Döbele, K. Hirsch, M. von Hellermann: "On Scattering Diagnostics with Periodically Pulsed Lasers to Follow the Continuous Evolution of Time Dependent Plasma Parameters", Plasma Physics 20, 241 (78)

/6/ F.N.H. Robinson: "Noise and Fluctuations in Electronic Devices and Circuits", Clarendon Press, Oxford, 1974

/7/ A.E. Barelli: "Improve avalanche-photodiode designs", Electronic Design 15, 68 (73)

/8/ M. Mattioli: "Incoherent Light Scattering From High Temperature Plasmas" EUR-CEA-FC-752, July 1974

Figure Captions

Fig. 1: 90° Thomson scattering geometry.

Fig. 2: 8° forward scattering geometry of laser beam and observation beam inside the torus.

Fig. 3: Definition of scattering volume by intersection of laser and observation beams (page 4).

Fig. 4: Necessary laser energy versus electron density for different laser types and scattering angles.

Fig. 5: Layout of 8° forward scattering experiment.

Fig. 6: Collection optics.

Fig. 7: Cross-section of laser and collection beams in the plane of mirror M2.

Fig. 8: Alignment scheme.

Fig. 9: Arrangement of spectral channels.

Fig. 10: Radiation power incident on the detector (page 26).

Fig. 11: Relative error of the temperature measurement for different numbers of equidistant spectral channels. The central channel is omitted.

Fig. 12: Relative error of the temperature measurement for different numbers of optimally distributed spectral channels. The central channel is omitted.

Fig. 13: Typical signal obtained with a fast detector (page 37).

Fig. 14: Integrated signal (page 38).

Fig. 15: Radial resolution as function of torus radius.

Fig. 16: Relative error of the temperature measurement due to finite solid angle observation optics.

Fig. 17: Shape of the scattered spectrum for different scattering angles (from /8/).

Fig. 18: Total half-width of the scattered spectrum versus the scattering angle.

Fig. 19: Shape of the scattered spectrum.

Fig. 20: Asymmetry of the scattered spectrum.

Fig. 21: Relativistic blue shift of the maximum of the scattered spectrum.

Fig. 22: Path of rays in the beam expanding telescope.

Fig. 23: Path of the alignment laser beam inside the torus.

Data sheet No. 1.

Data sheet No. 2.

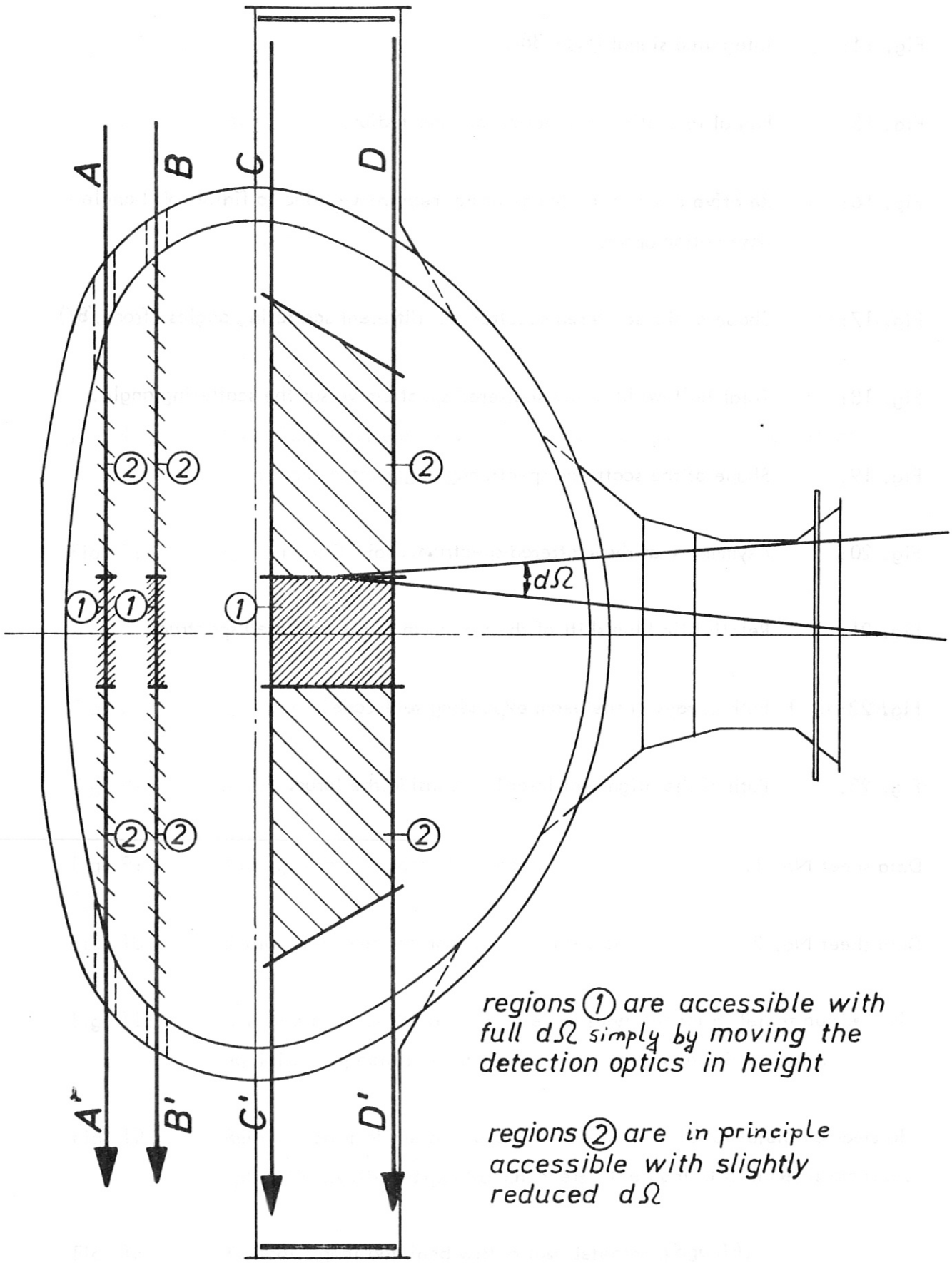

Fig. 1: 90° Thomson scattering geometry.

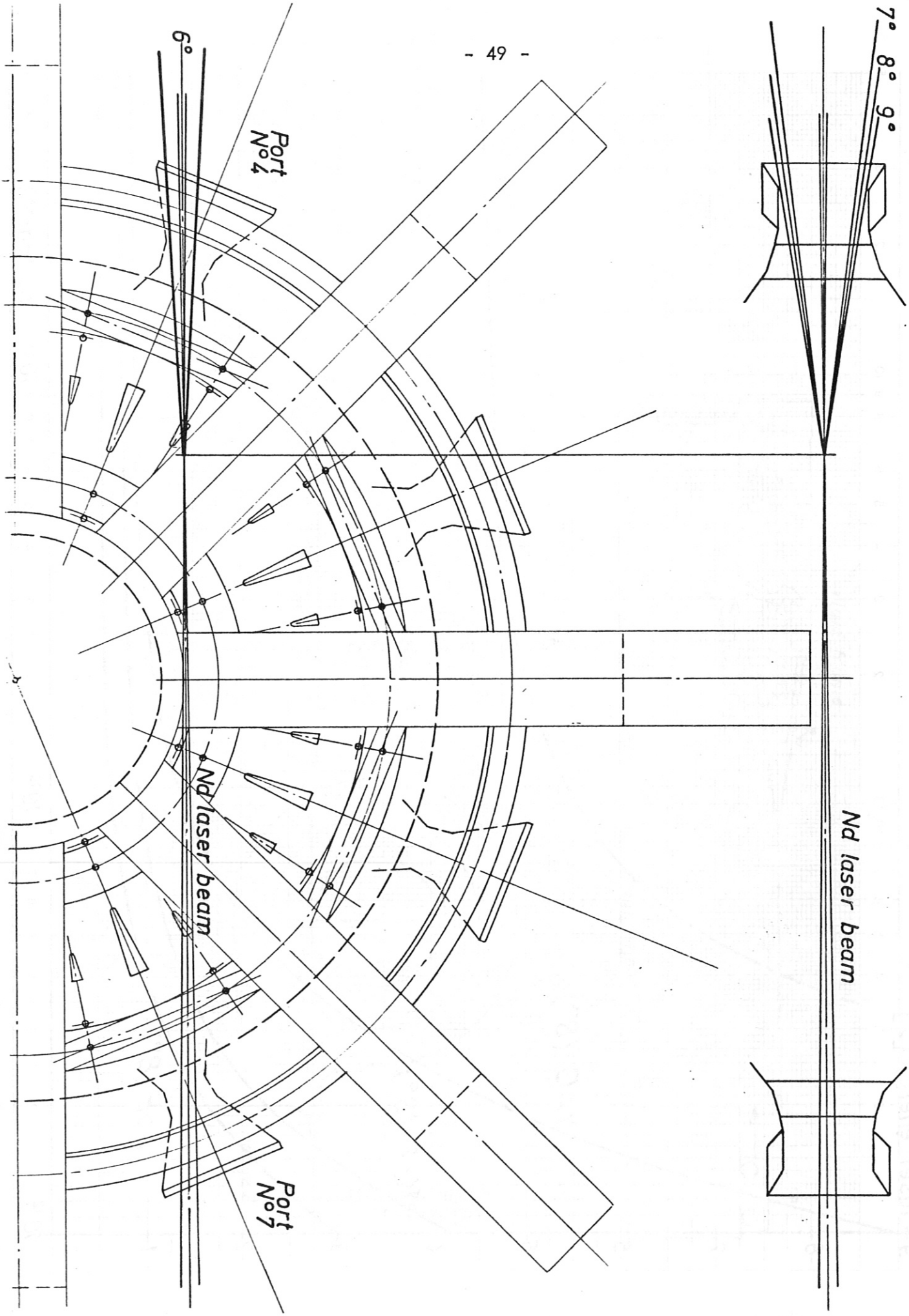

Fig. 2: 8° forward scattering: geometry of laser beam and observation beam inside the torus.

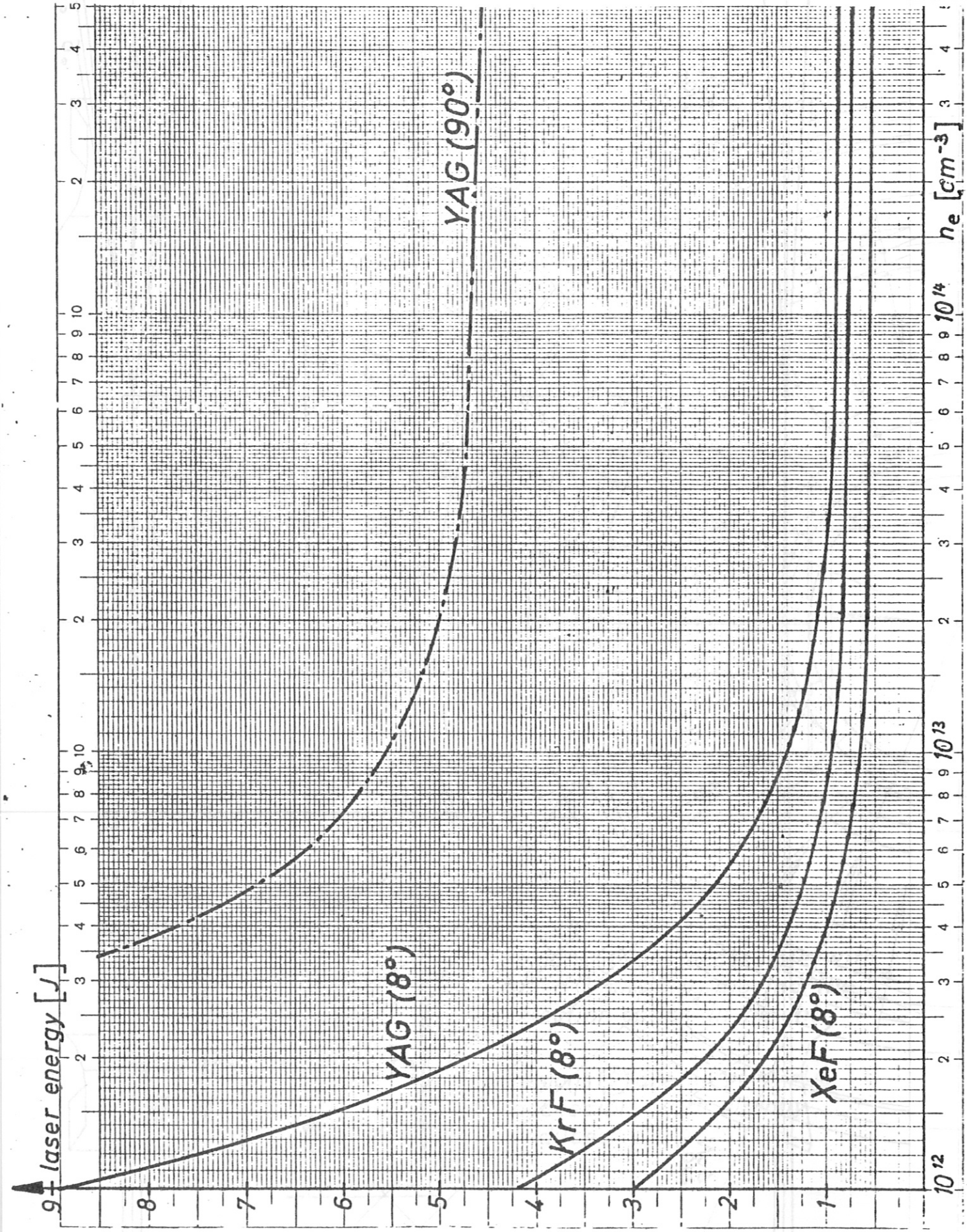

Fig. 4: Necessary laser energy versus electron density for different laser types and scattering angles.

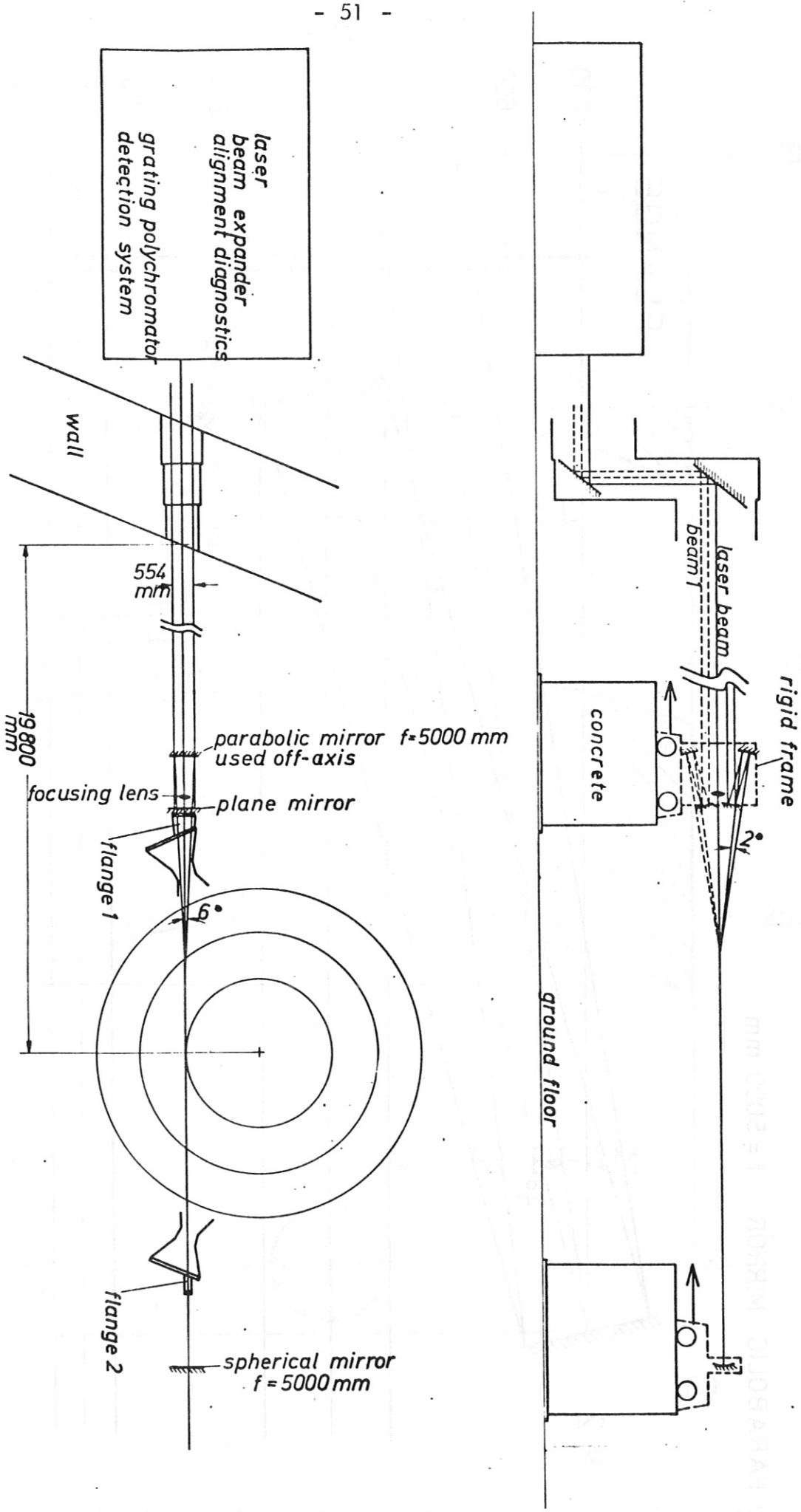

Fig. 5: Lay-out of 8° forward scattering experiment.

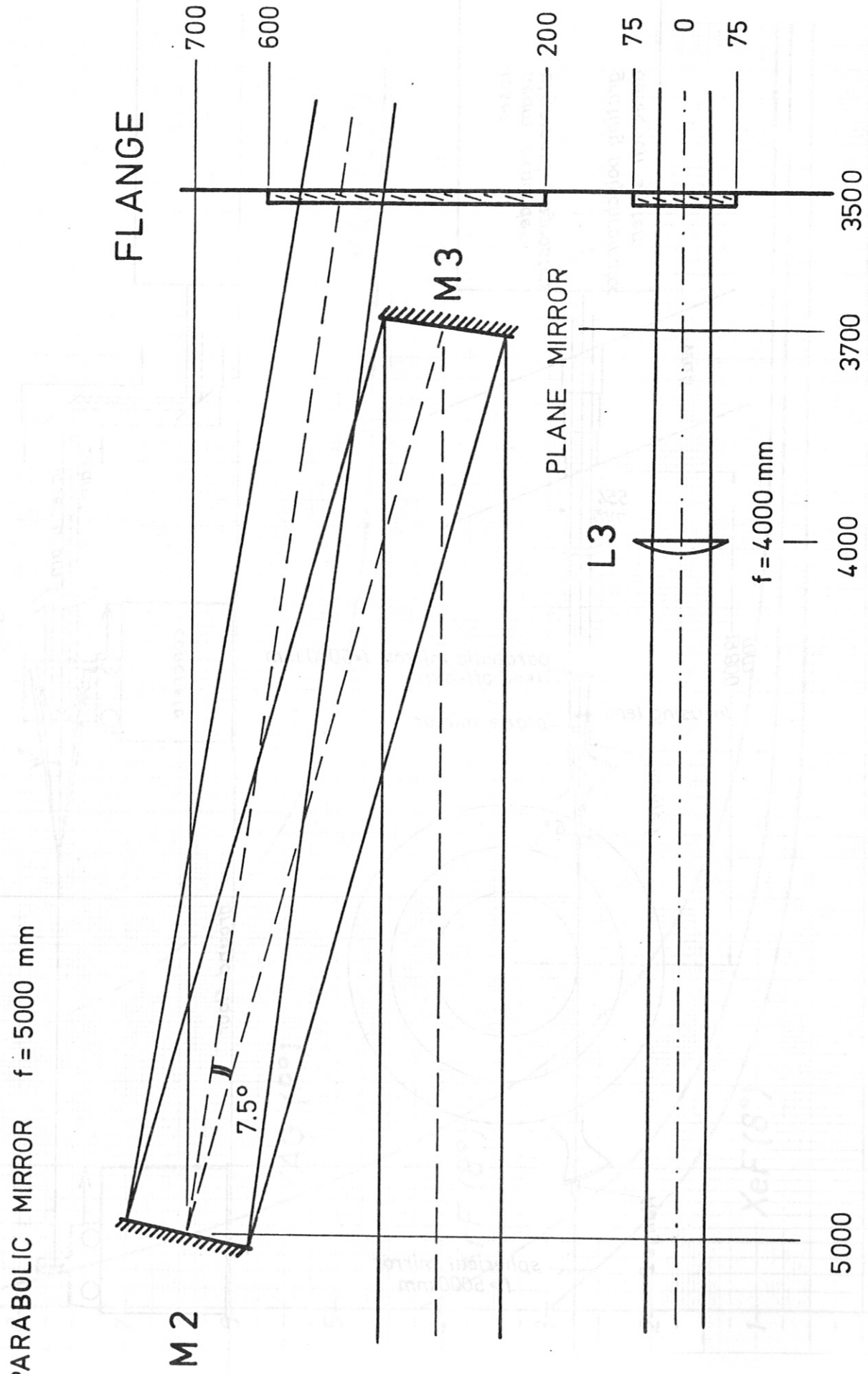

Fig. 6: Collection optics.

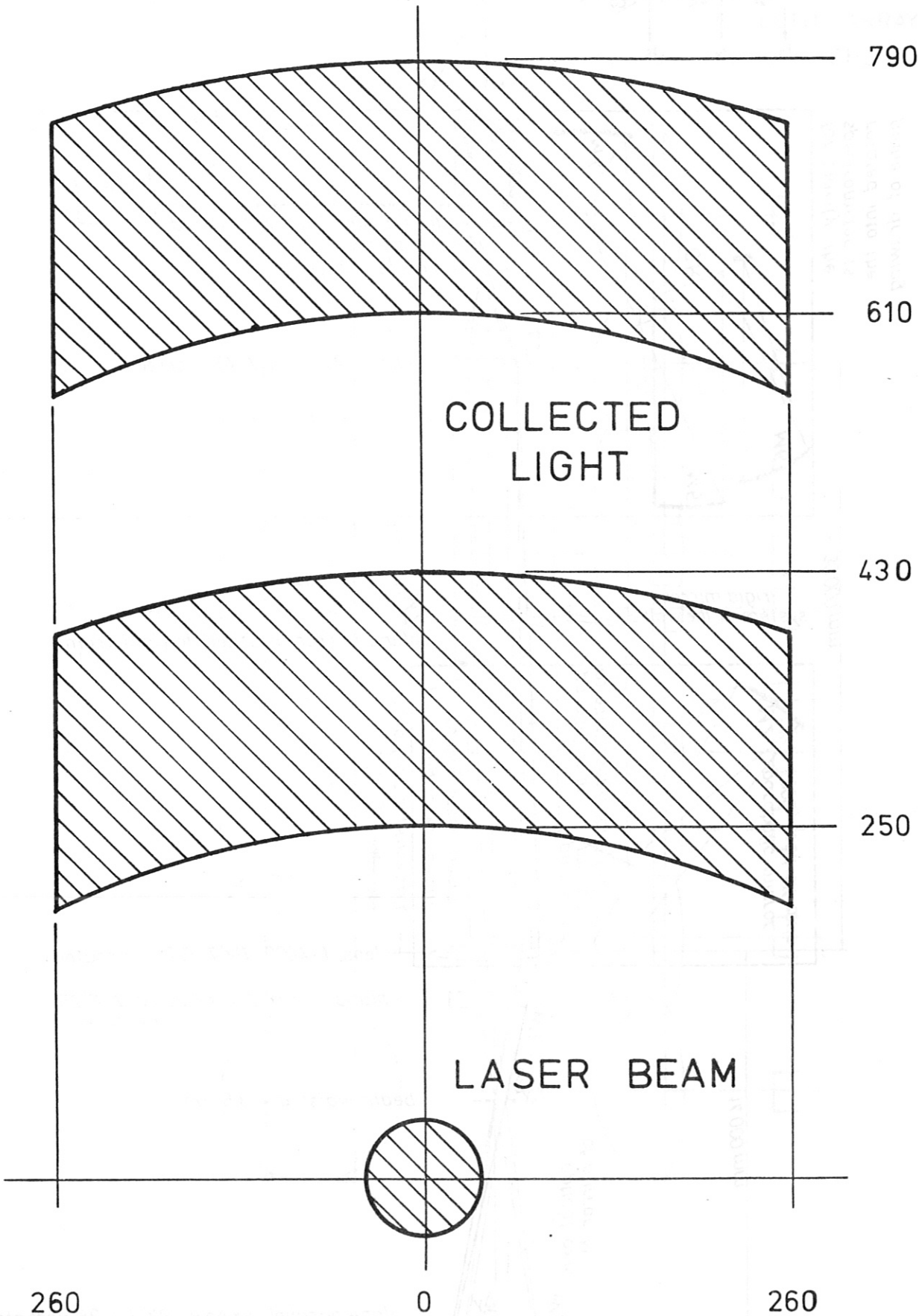

Fig. 7: Cross-section of laser and collection beams in the plane of mirror M2.

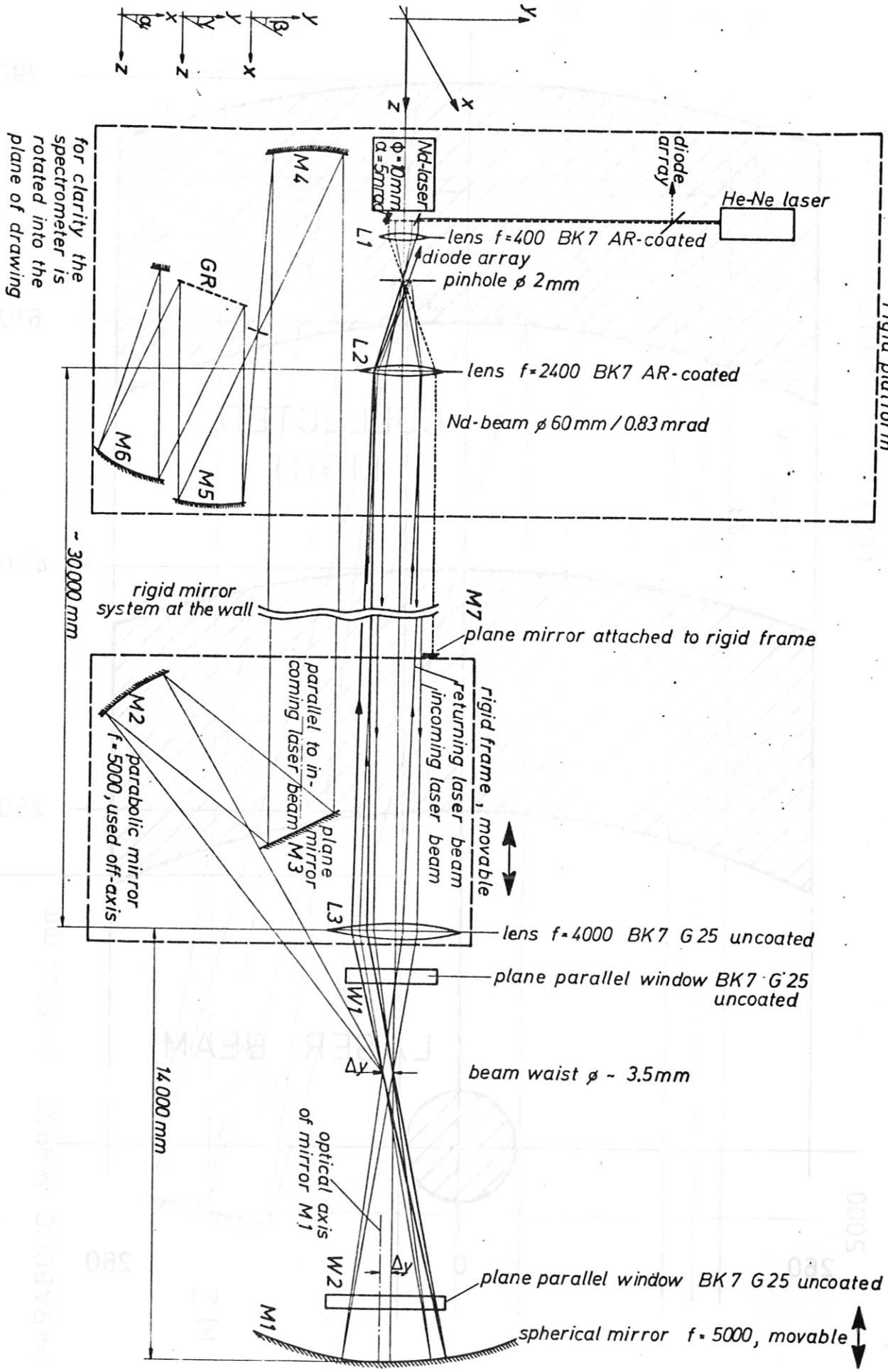

Fig. 8: Alignment scheme.

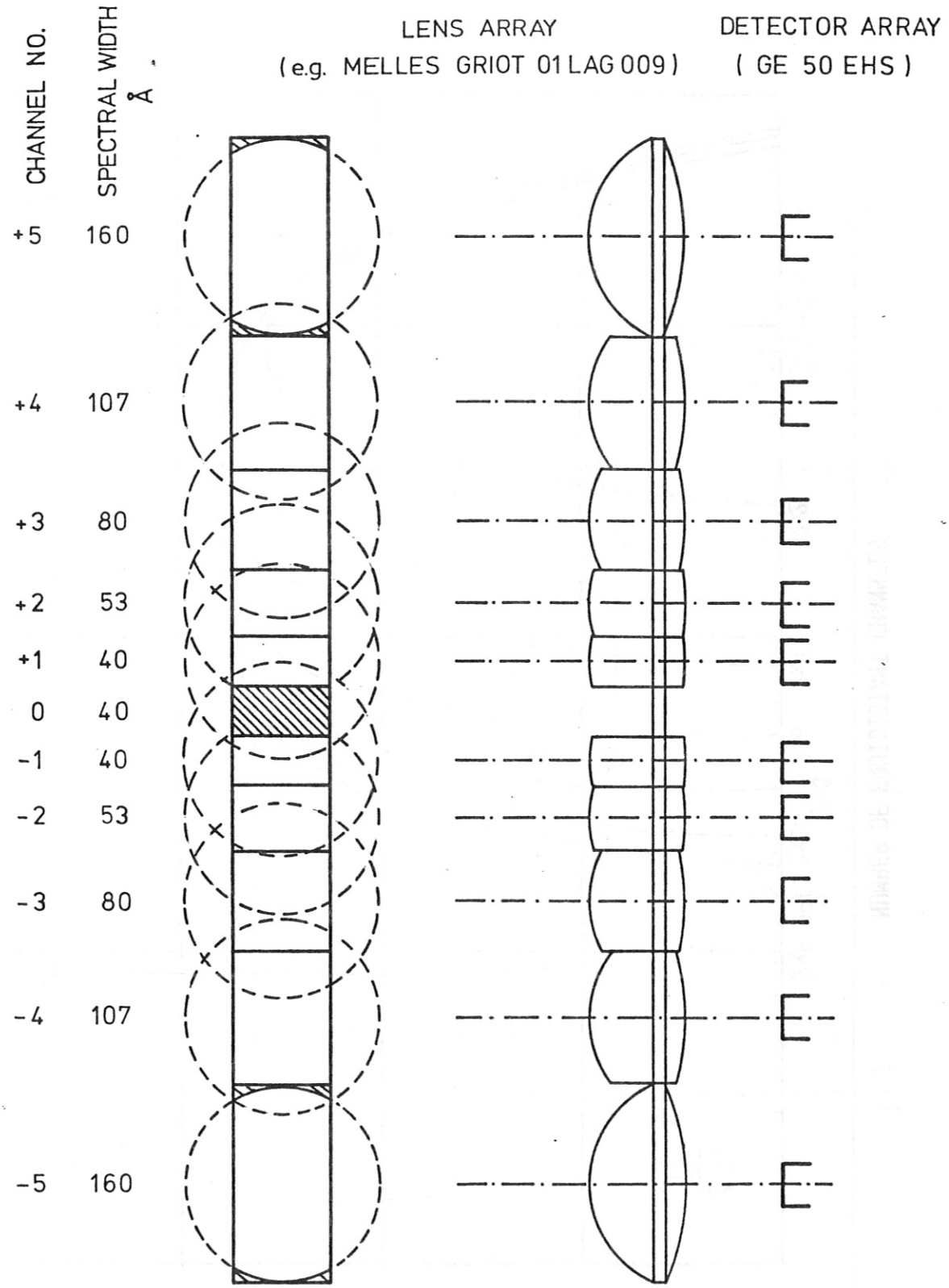

Fig. 9: Arrangement of spectral channels.

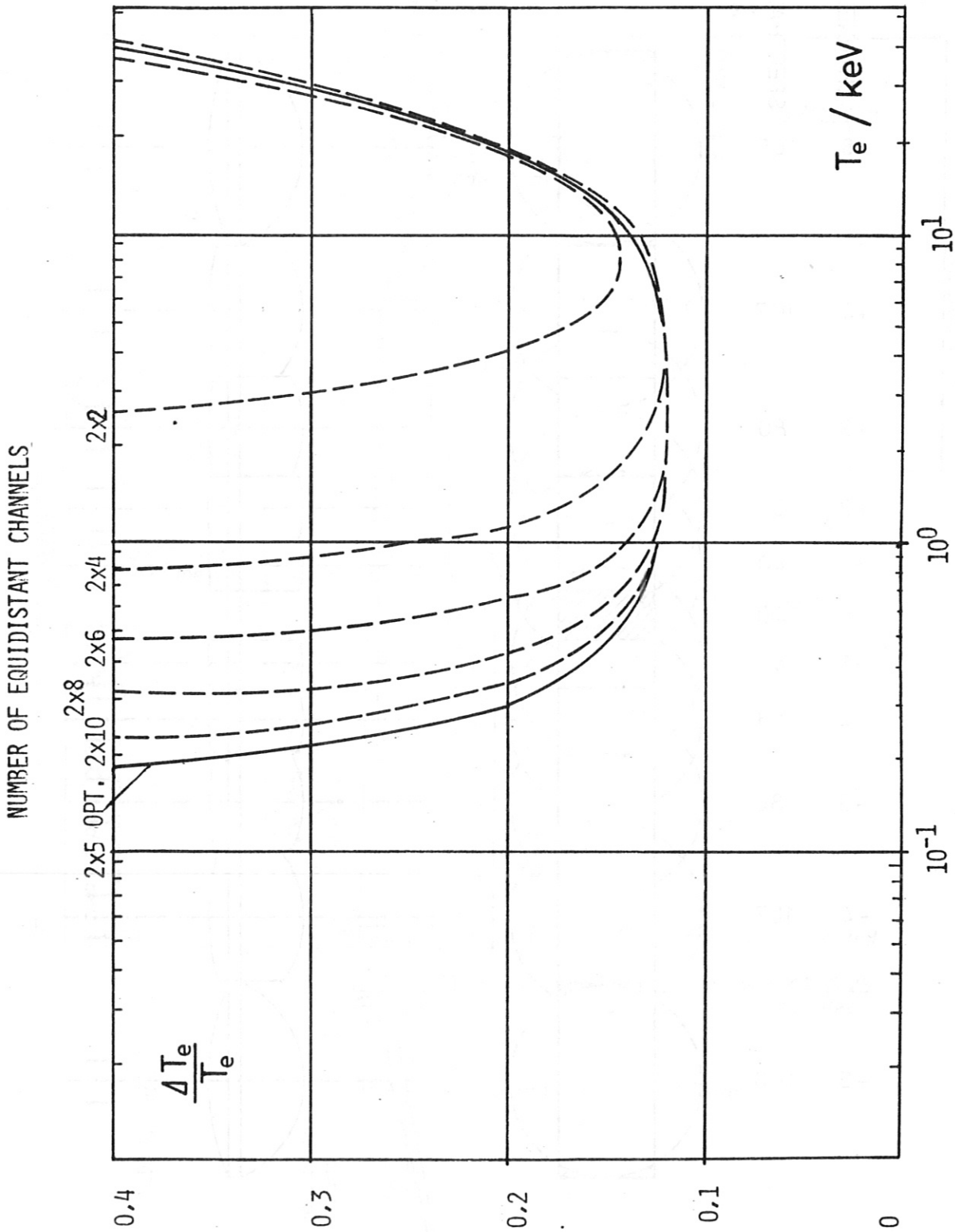

Fig. 11: Relative error of the temperature measurement for different numbers of equidistant spectral channels. The central channel is omitted.

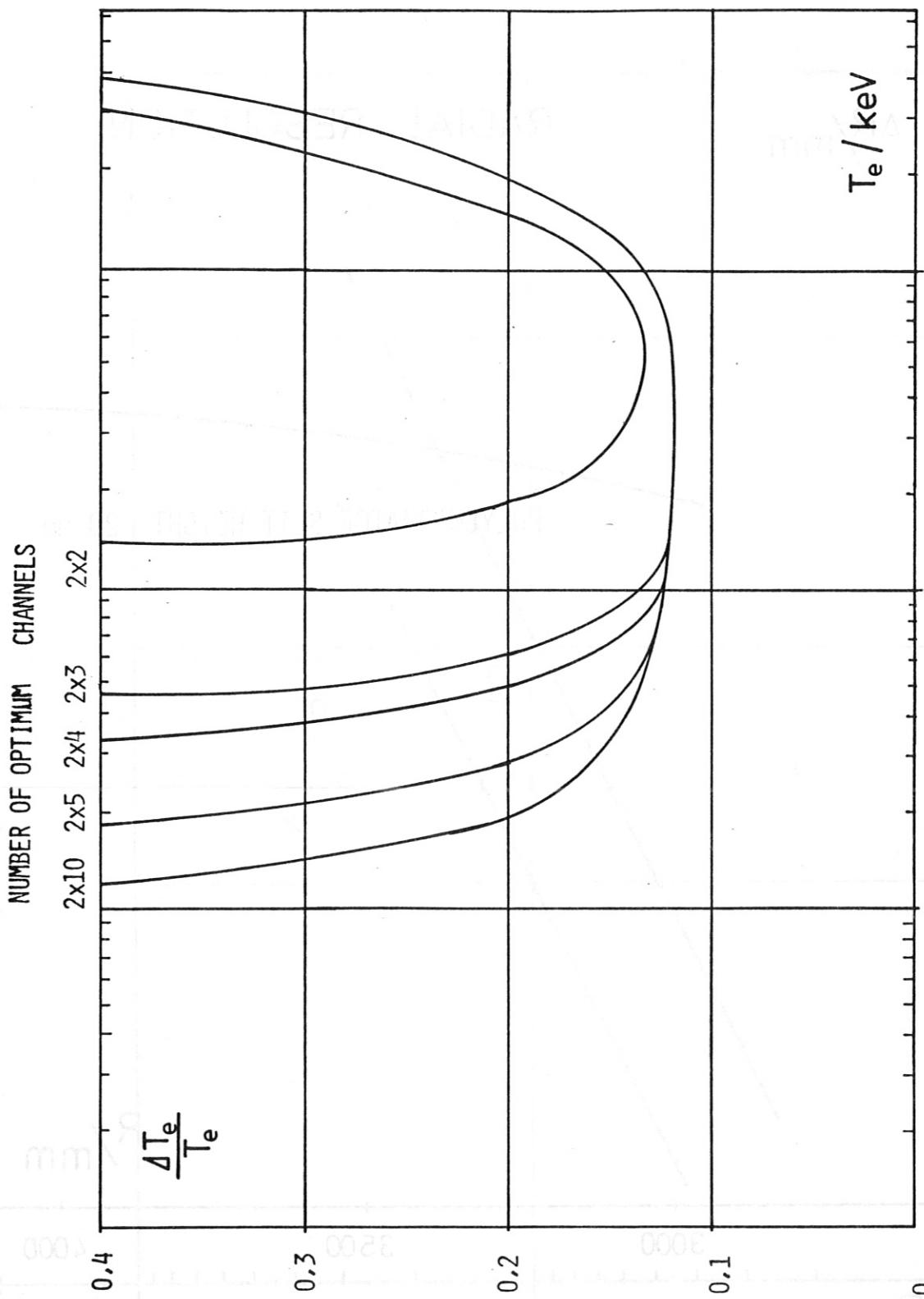

Fig. 12: Relative error of the temperature measurement for different numbers of optimum distributed spectral channels. The central channel is omitted.

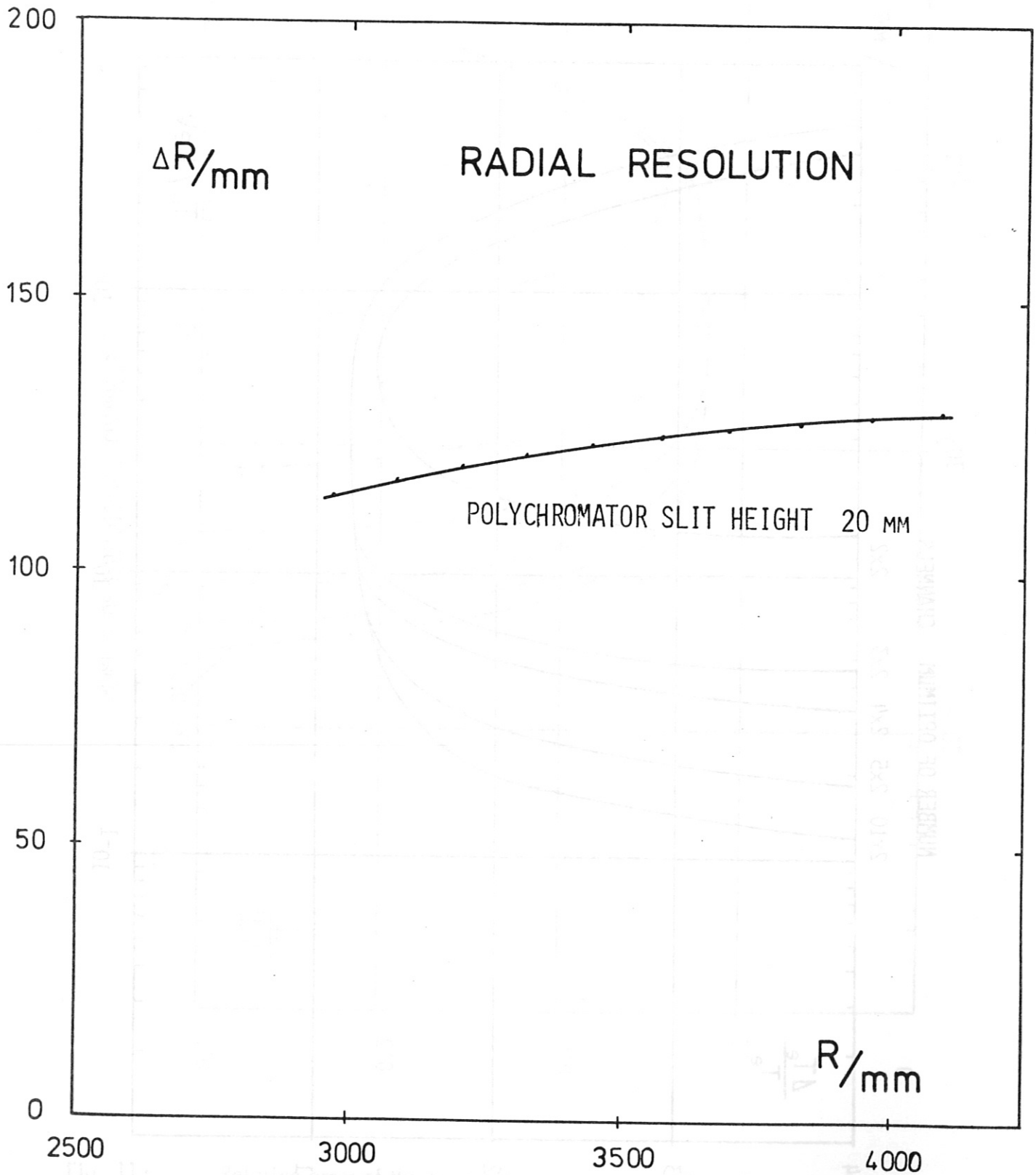

Fig. 15: Radial resolution as function of torus radius.

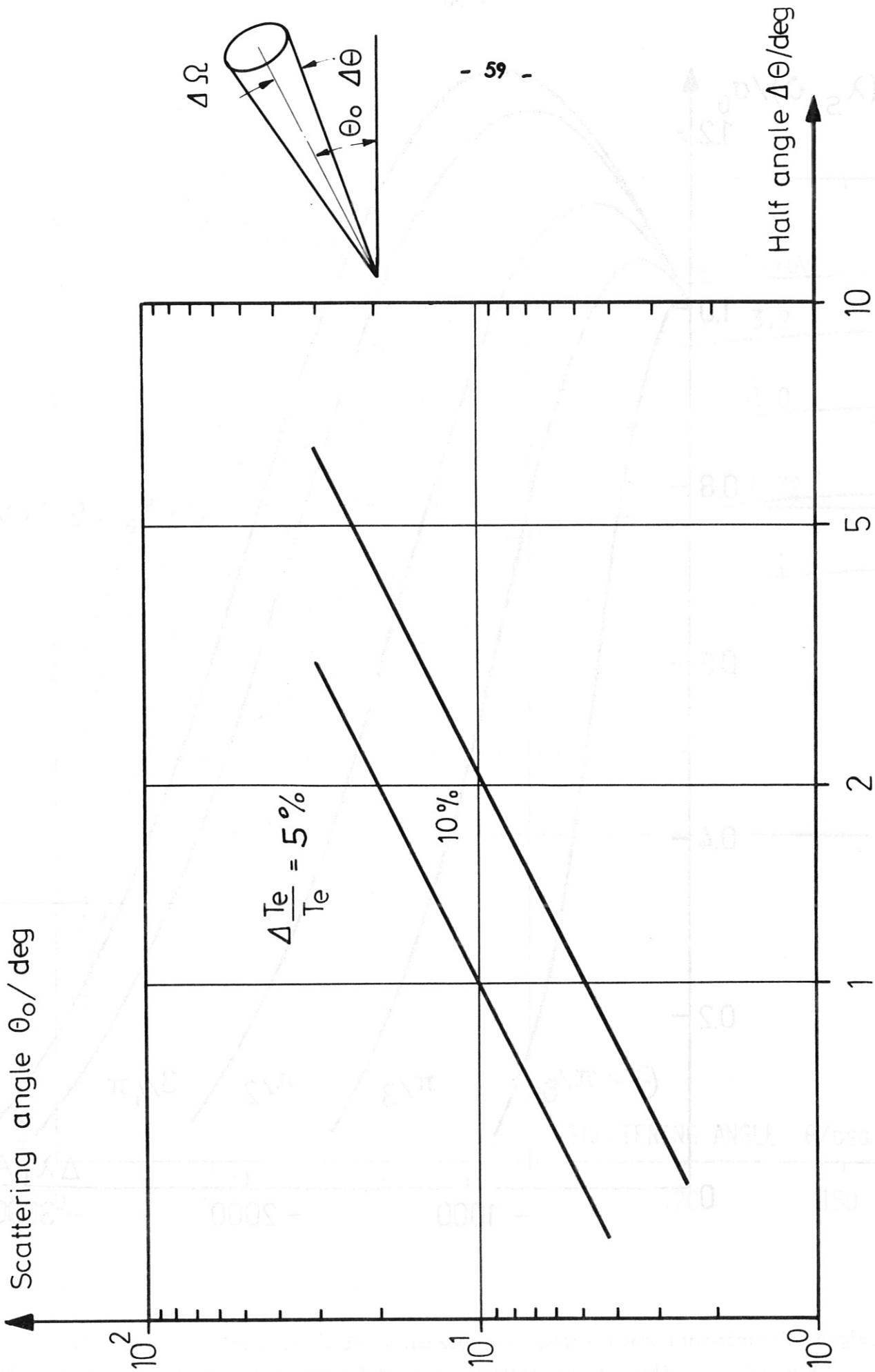

Fig. 16: Relative error of the temperature measurement due to finite solid angle observation otpics.

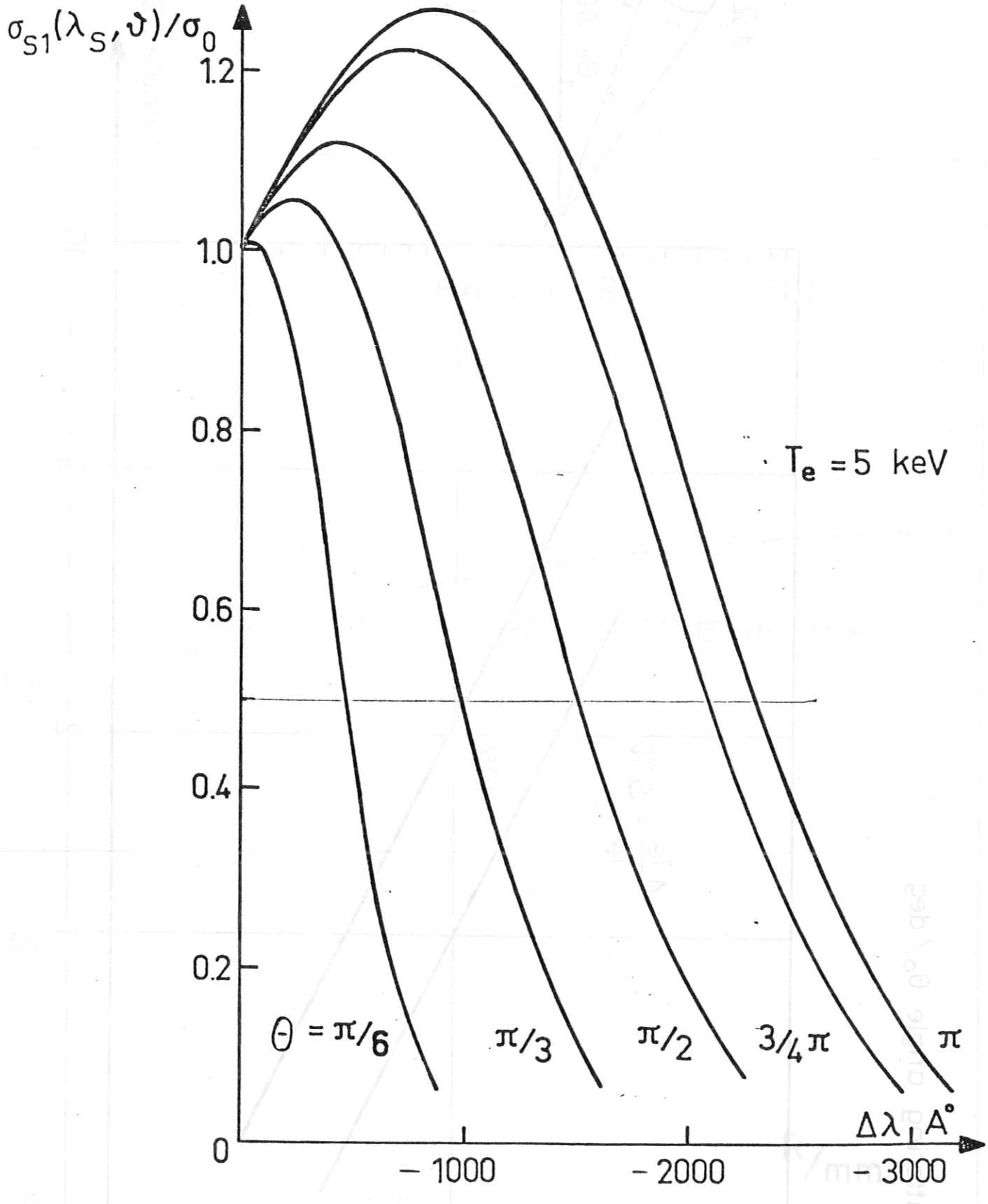

Fig. 17: Shape of the scattered spectrum for different scattering angles (from /8/).

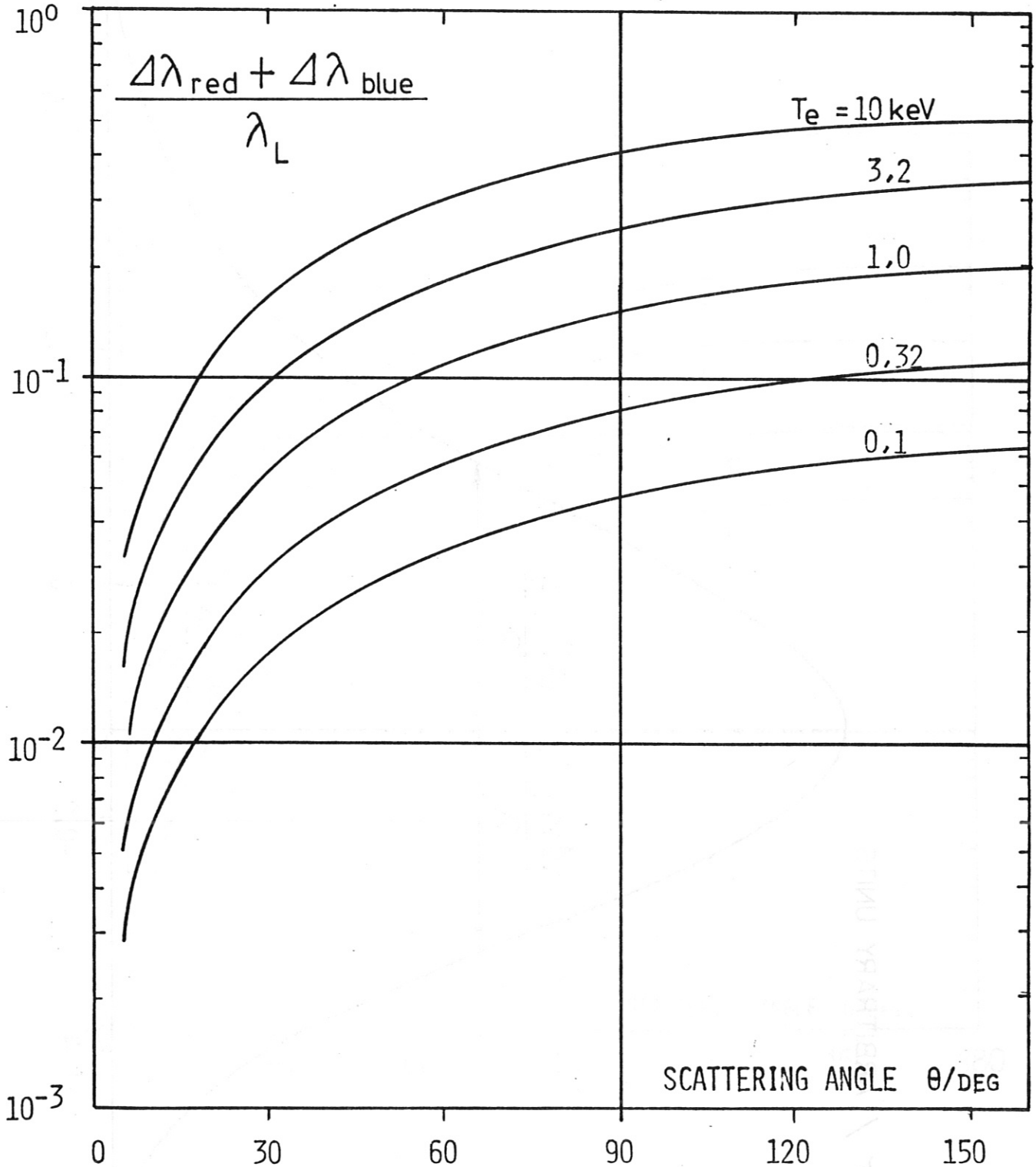

Fig. 18: Total half width of the scattered spectrum versus the scattering angle.

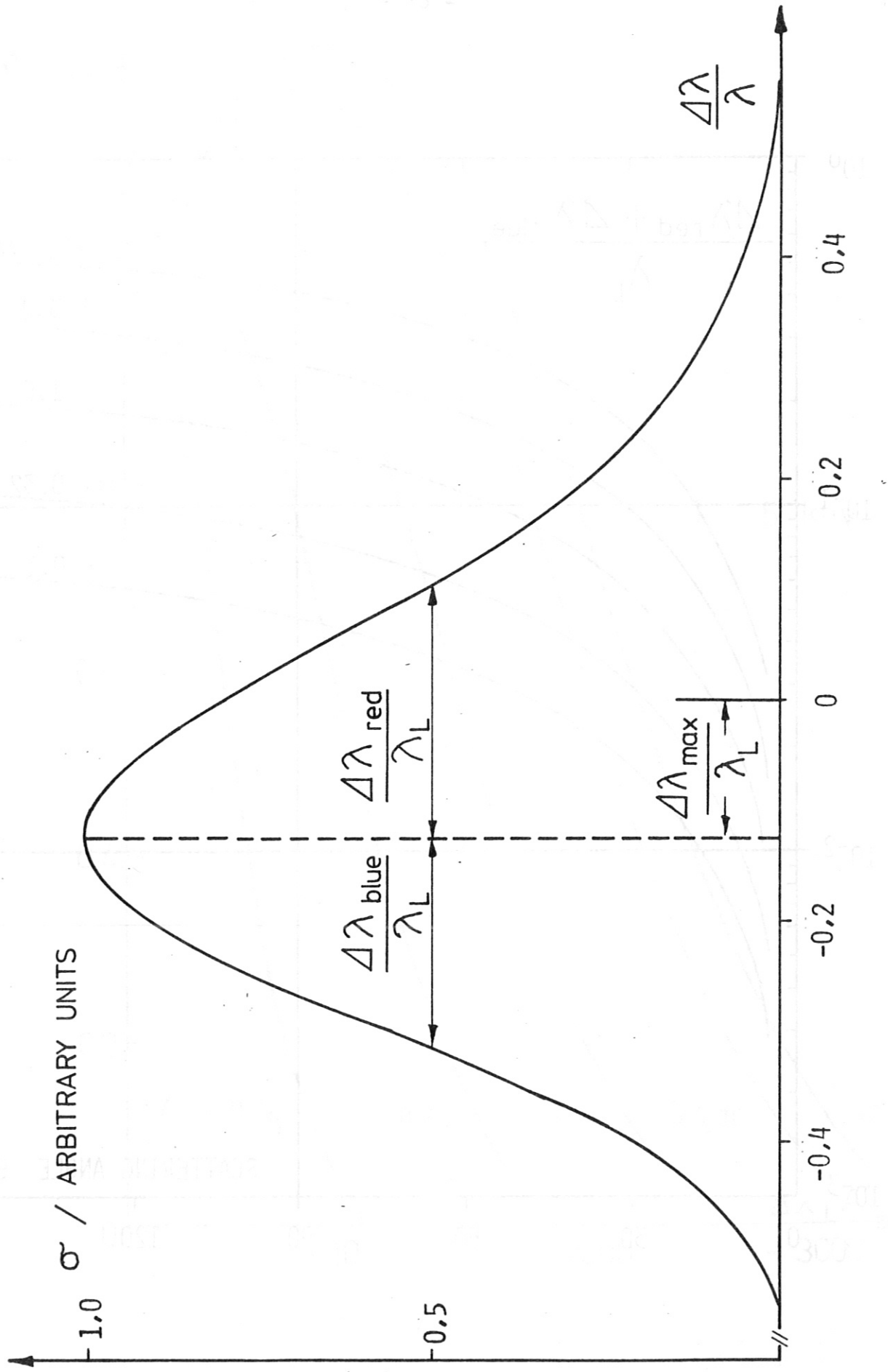

Fig. 19: Shape of the scattered spectrum.

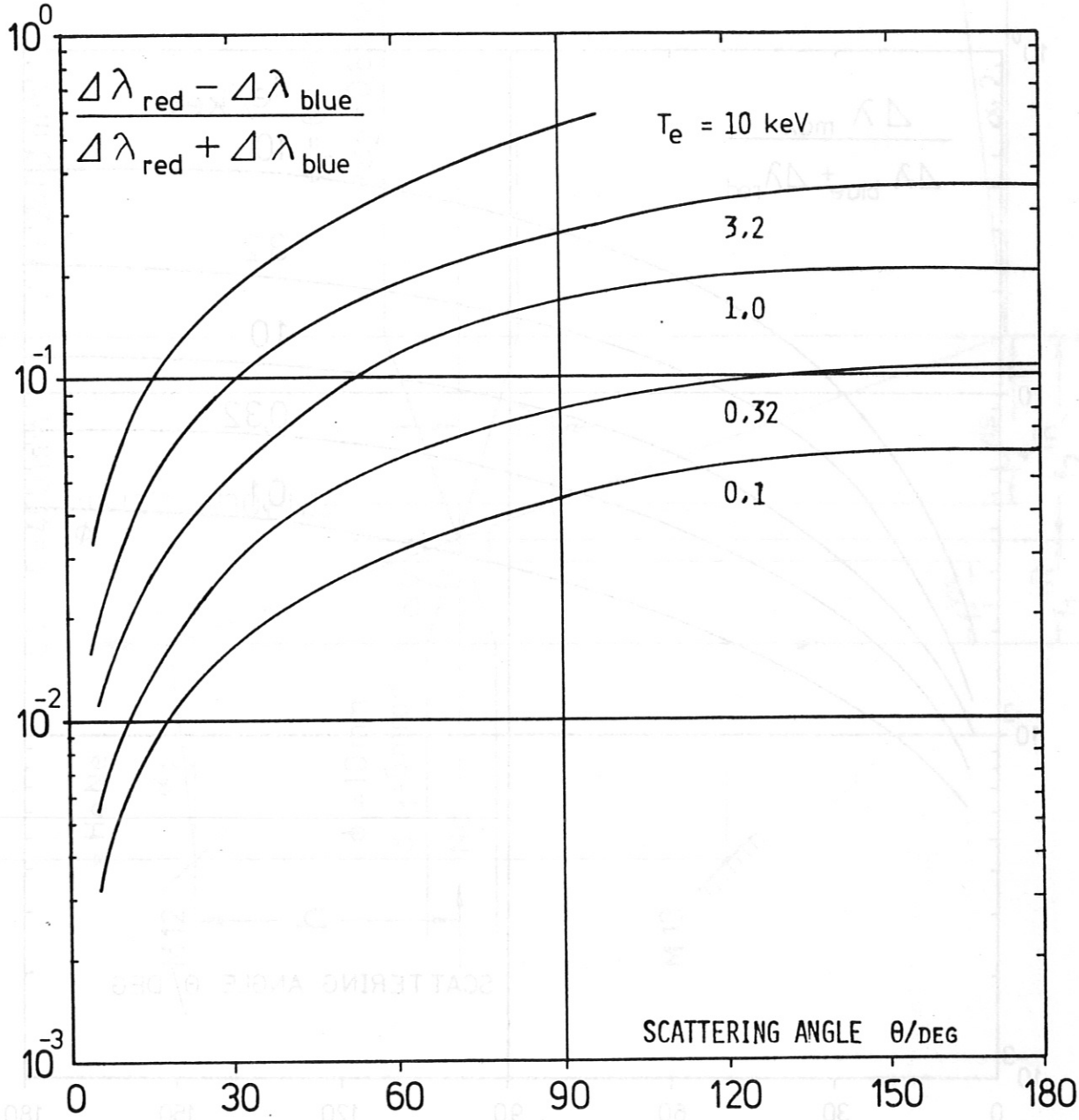

Fig. 20: Asymmetry of the scattered spectrum.

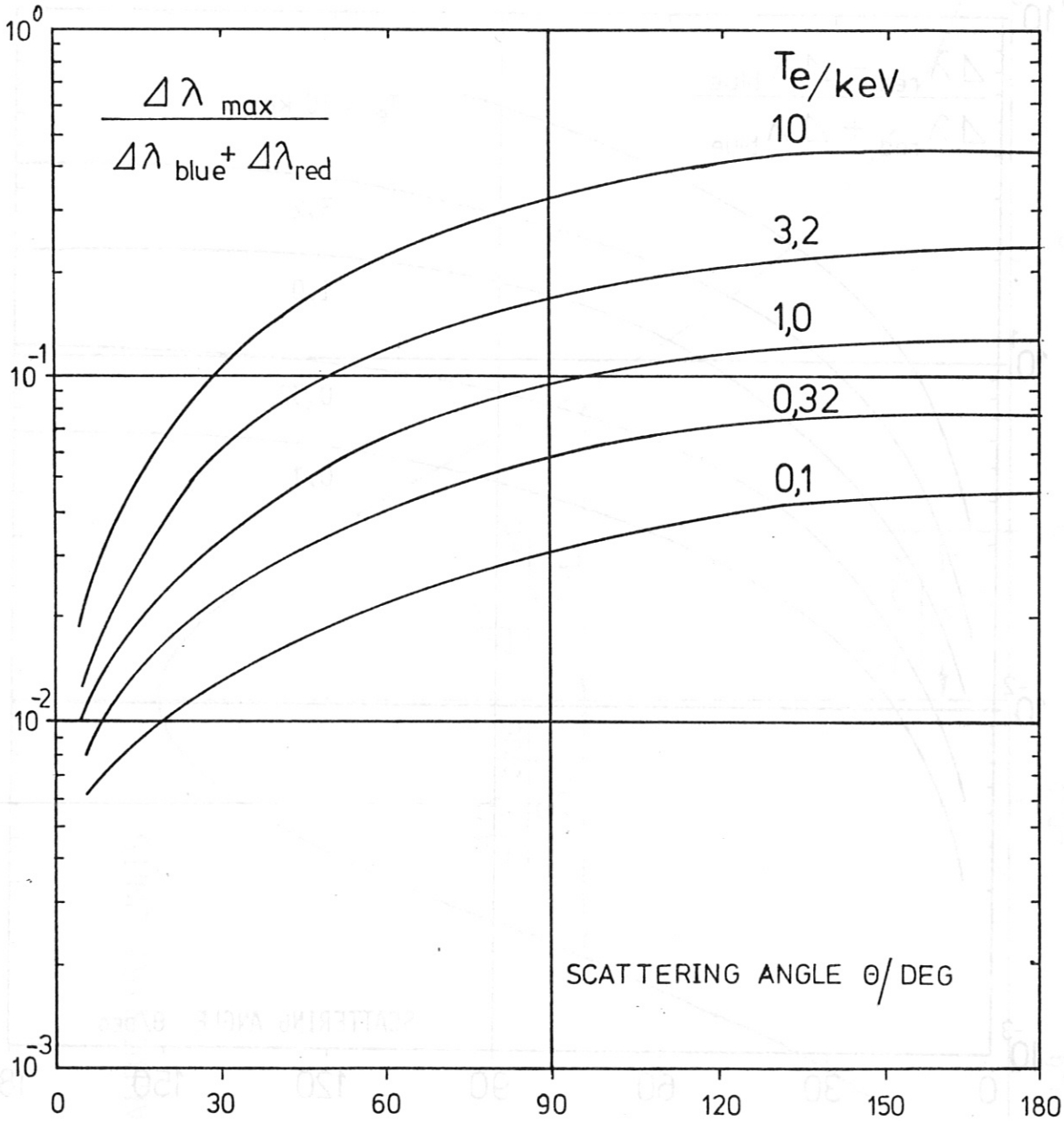

Fig. 21 : Relativistic blue shift of the maximum of the scattered spectrum.

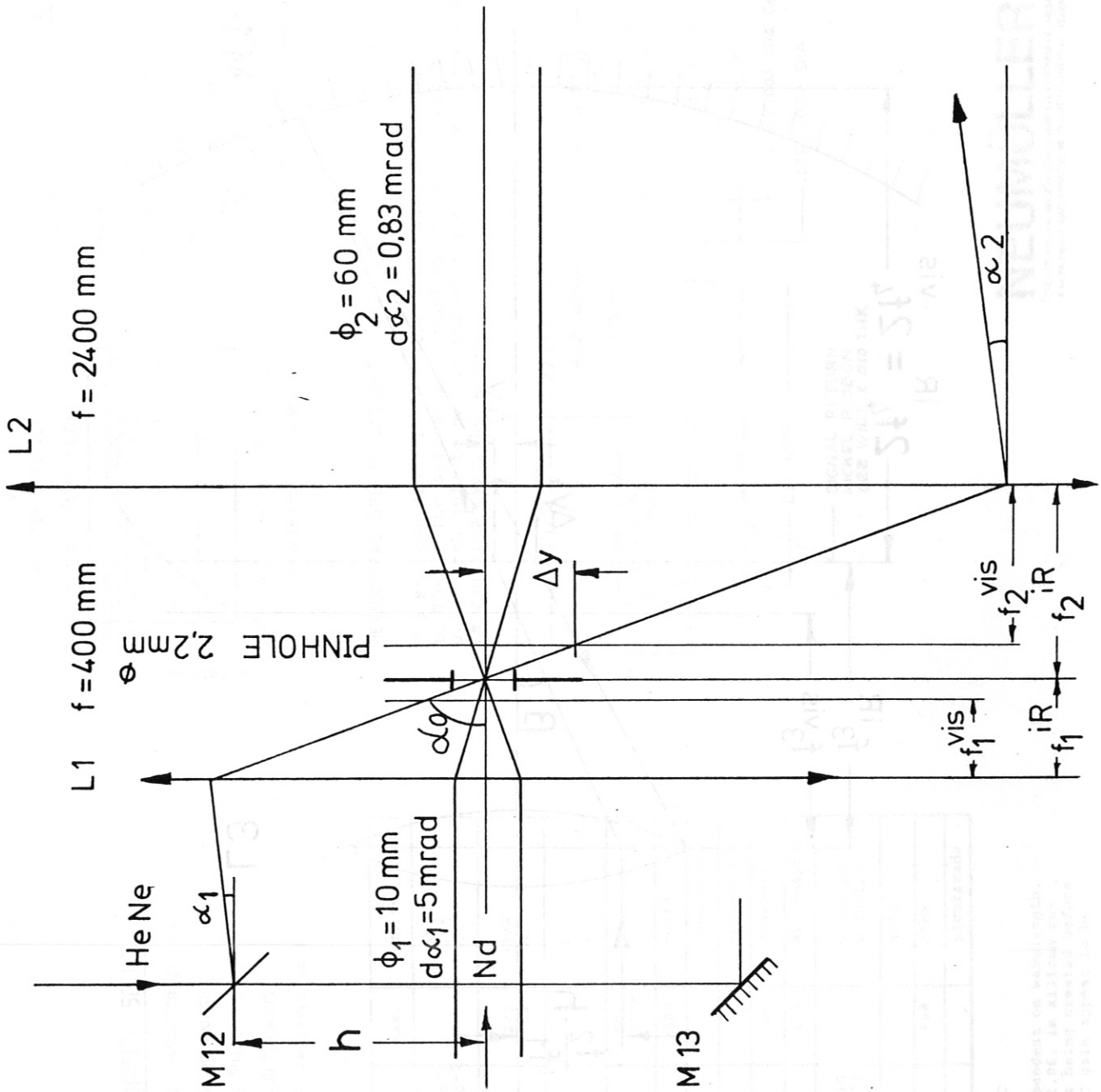

Fig. 22: Path of rays in the beam expanding telescope.

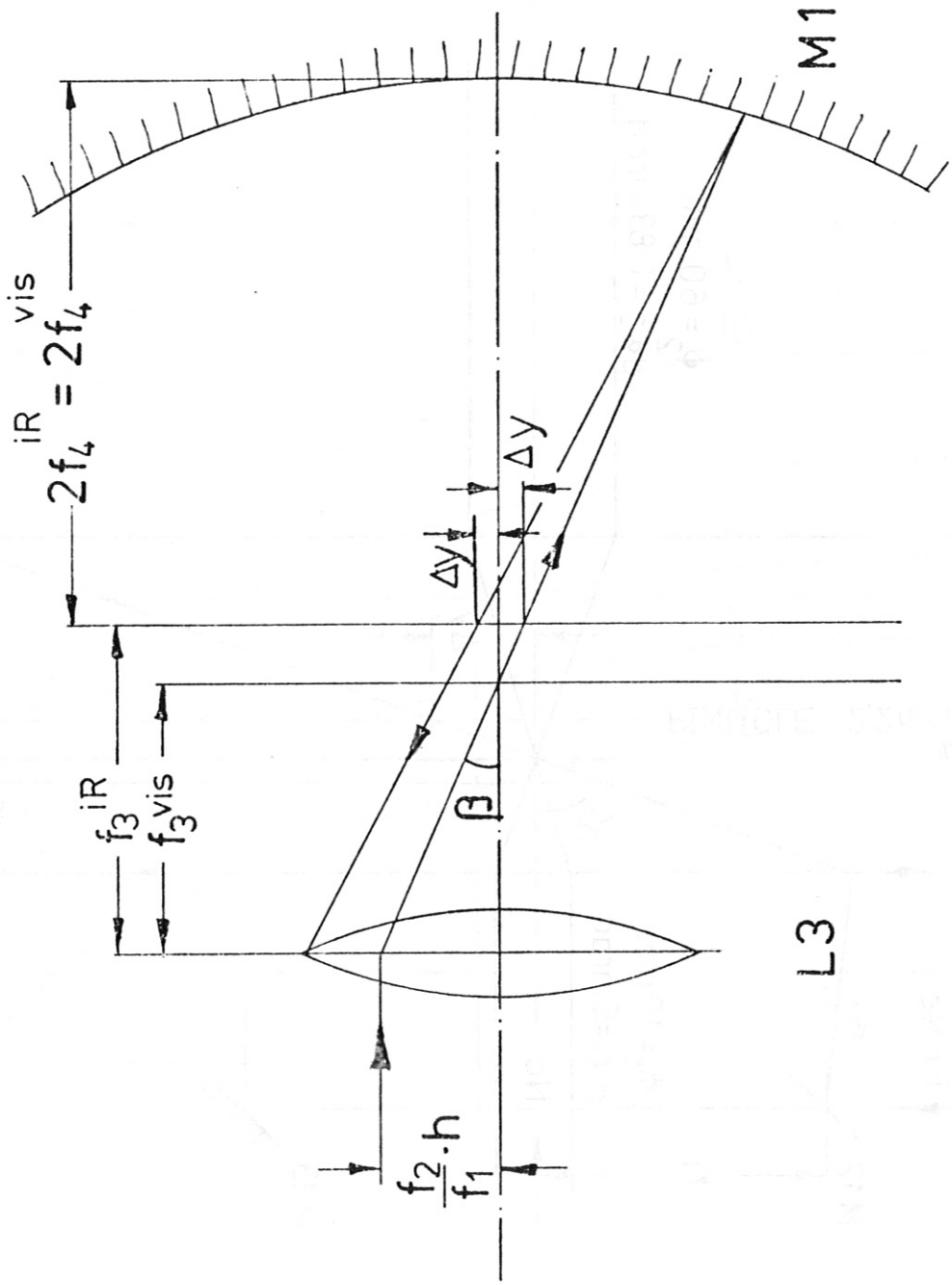

Fig. 23: Path of the alignment laser beam inside the torus.

SPACE TECHNOLOGY PRODUCTS

TECHNICAL INFORMATION

SILICON AVALANCHE PHOTODIODES 50EHS

THE 50EHS SILICON AVALANCHE PHOTODIODE IS CHARACTERIZED BY:

- LARGE ACTIVE AREA
- FAST RESPONSE
- UNIFORM HIGH GAIN
- LOW NOISE
- HIGH QUANTUM EFFICIENCY BEYOND 1.06 MICRONS

IT IS PRIMARILY INTENDED FOR DETECTION OF LOW LEVEL FAST LASER PULSES AT 1.06 AND 0.9 MICRONS.

ELECTRO-OPTICAL SPECIFICATIONS

	Min.	Typ.	Max.	Units
Active Area (dia) (area)		0.125 1.22×10^{-2} 7.8×10^{-2}		in in^2 cm^2
Responsivity (0.90μ, 0.98Va, 40ns) (1.06μ, C.98V_a, 20ns)	80 20	110 25	275 60	A/W A/W
Quantum Efficiency (0.90μ, 0.25V_a, 40ns) (1.06μ, 0.25V_a, 20ns)		75 30		% %
Gain (0.90μ, 0.98V_a, 40ns) (1.06μ, 0.98V_a, 20ns)	150 75*	200 100*	500 250*	
Avalanche Voltage, V_a	1800	2200	2600	volts
Rise Time		3		nanosecond
Fall Time		12		nanosecond
Gain BW Product	10	20	30	gigahertz
Dark Current** (0.98V_a 25°C)		0.7	1.5	microamperes
Noise (NEP) (0.90μ, 0.98V_a, 40ns) (1.06μ, 0.98V_a, 20ns)		5×10^{-15} 2×10^{-14}		W Hz-1/2 W Hz-1/2
Temp.Coeff. of Va		0.11		%/°C
Series Resistance		400	600	ohms
Capacitance		6		picofarads

Operating case temperature: -40 to 70°C
Storage temperature: -65 to 150°C

* The electron multiplication is not dependent on wavelength. However, the long absorption length of 1.06μ in silicon results in only half of the photoelectrons being created before the gain region which makes the measured gain appear to be lower by one half.

**In silicon the dark current doubles for each 10°C rise in temperature.

Data sheet No. 1

TYPICAL CHARACTERISTICS

QUANTUM EFFICIENCY VS WAVELENGTH

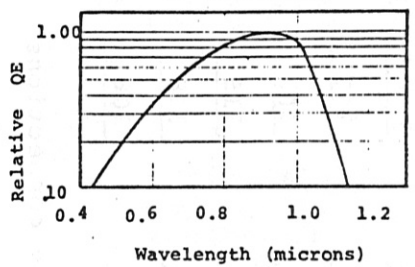

GAIN VS BIAS

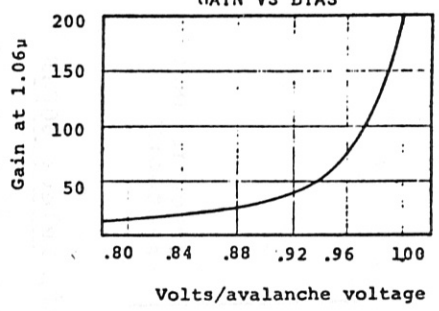

MECHANICAL SPECIFICATIONS

The silicon diode is hermetically packaged in a can similar to TO-5. The silicon is bonded to the header which has a 0.125 inch hole to expose the active area. No glass window is required over the diode.

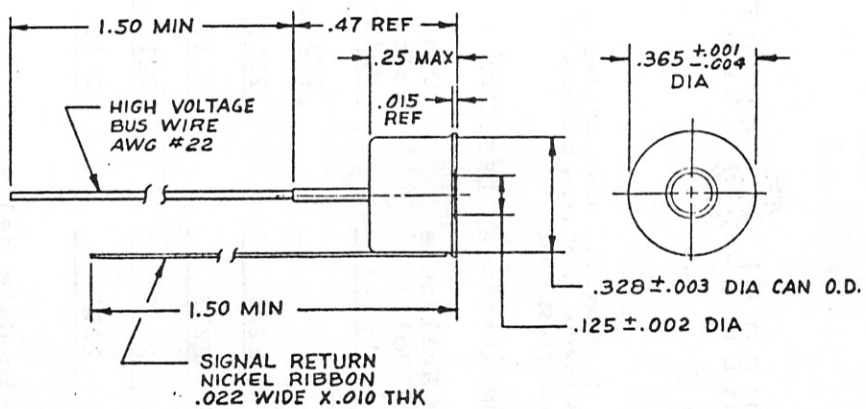

GENERAL ELECTRIC

GENERAL ELECTRIC COMPANY ... KING OF PRUSSIA PARK, P.O. BOX 8439
PHILADELPHIA, PENNSYLVANIA 19101, Phone (215) 962-4000
TELEX: 846413, KING OF PRUSSIA, PA.

SPACE TECHNOLOGY
PRODUCTS

SILICON AVALANCHE DETECTOR - DATA SHEET - MODEL Select 50EHS

Serial Number	Avalanche Voltage Volts	Test Voltage Volts	Leakage Current μ Amps	Resp. A/W @ 0.9μ	$\frac{I_L}{\text{Resp.}}$ 10^{-9}
CCD	2223	2203	.12	107	1.12
JJU	2229	2209	.10	103	.9
JJV	2237	2217	.13	115	1.13
JJW	2235	2215	.18	128	1.4
JJX	2239	2219	.19	108	1.7

The schematic data below is useful to describe the connections and possible circuits.

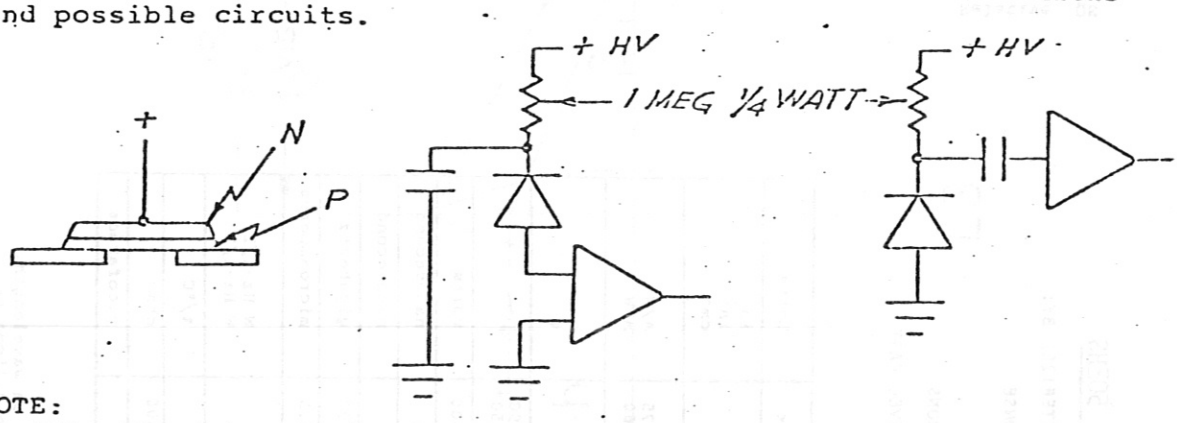

NOTE:

(1) The detector is free of plasma noise events when operated below the rated avalanche voltage.
(2) Temperature coefficient of avalanche is approximately 2.16V/°C
(3) The depletion region is formed at 500V. Here the gain is unity.
(4) The gain increases exponentially as a function of voltage with the gain highest when operated close to avalanche.

CAUTION:

The diode is mounted to the gold header with a silver conductive epoxy. Do not apply any pressure to the surface of the diode. The TO-5 can and the header are joined with a silver conductive epoxy. Do not apply any pressure to the header. Apply a heat sink to the high voltage pin when soldering to the high voltage lead.